Ligand-Enforced Geometries and Associated Reactivity in P-Block Compounds

Tyler J. Hannah[a] and Saurabh S. Chitnis[a,*]

[a]Department of Chemistry, Dalhousie University, 6274 Coburg Road, Halifax, NS, B3H 4R2, Canada
*Corresponding author: saurabh.chitnis@dal.ca

TOC Figure and Text:

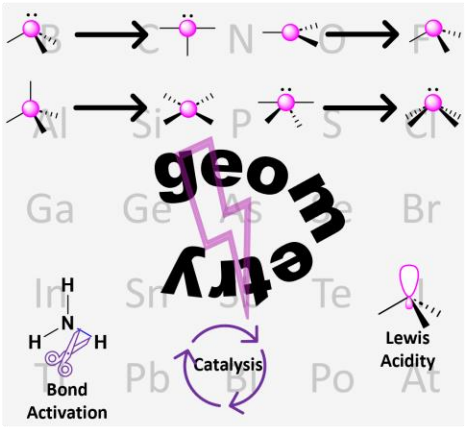

This review presents a group-wise summary of ligand enforced non-VSEPR geometries in compounds of the p-block elements and discusses the emergent consequences for reactivity.

Abstract

The geometry at an element centre can generally be predicted based on the number of electron pairs around it using valence shell electron pair repulsion (VSEPR) theory. Strategies to distort p-block compounds away from these predicted geometries have gained considerable interest due to the unique structural outcomes, spectroscopic properties or reactivity patterns engendered by such distortion. This review presents an up-to-date group-wise summary of this exciting and rapidly growing field with a focus on understanding how the ligand employed unlocks structural features, which in turn influences the associated reactivity. Relevant geometrically constrained

compounds from groups 13-16 are discussed, along with selected stoichiometric and catalytic reactions. Several areas for advancement in this field are also discussed. Collectively, this review advances the notion of geometric tuning as an important lever, alongside electronic and steric tuning, in controlling bonding and reactivity at p-block centres.

Introduction

Understanding the connection between structure and function is a key aspect of inquiry in any physical science. In chemistry, this pursuit involves exploring how structure at molecular, macromolecular, or supramolecular length scales influences the functionally-relevant properties of a chemical entity, which may be intrinsic (e.g. magnetism) or extrinsic (e.g. reactivity towards other species).

An important conceptual achievement in molecular p-block chemistry was the development in the 1950s of the valence shell electron pair repulsion (VSEPR) model by Gillespie, Nyholm, Sidgwick, Powell and others.[1-3] The fundamental tenet of this model is the deterministic role that electron-electron repulsion plays in the arrangement of substituents around a central atom. Walsh showed in the 1950s that wavefunction methods based on qualitative molecular orbital (MO) theory[4] can also correctly predict the most stable structure of molecules.[5-11] Notably Walsh also arrived at the conclusion that "the shape of a molecule in its ground state depends primarily on the number of valency electrons."[5] This qualitative MO treatment was further cemented by formal quantitative approaches in 1970s by Allen, but its overall conclusions regarding the prime role of electron pair count were retained.[12] Further refinements to the VSEPR model in light of apparent exceptions led to recognition of the influence of ligand close packing [13, 14] and Jahn-Teller distortions.[15-17] The VSEPR notion of repulsion was formalized in the 1980s in real space by Bader's quantum theory of atoms in molecules (QTAIM), which described how volumes of electron-densities are deformed by interaction with one another under the directing influence of the Pauli exclusion principle.[13, 14] This is perhaps best encapsulated in Bader's bold proclamation that "the VSEPR model is now reduced to a single postulate, namely, that the most stable molecular geometry of a molecule AX_n corresponds to maximizing the separations between the local maxima in the valence shell of charge concentration of the atom A as defined by the Laplacian of the charge density".[18] That the general prediction of an intuitive VSEPR model for main group compounds re-emerge relatively unscathed from increasingly stricter quantitative treatments by QTAIM and MO analyses make it a key conceptual framework for understanding molecular shapes, and a mainstay of introductory chemistry curricula worldwide.[1, 19]

The ability to understand and predict structure naturally prompts efforts to exert control over it, leading to the quest for VSEPR non-compliant molecules: those for which the observed geometry differs from the one predicted by simply counting the number and types of electron pairs in the first coordination sphere around a central element. Besides the intellectual challenge of devising synthetic routes towards unusual molecules, the chief motivation behind accessing VSEPR non-compliant main group molecules is to provide molecular and electronic structure models for otherwise fleeting reaction intermediates or dynamic molecular processes (e.g. inversion). Non-classical geometries also generate frontier molecular orbital manifolds that are distinct from classical ones, enabling new modes of stoichiometric or catalytic reactivity.

One methodology for distorting molecular structures is the use of multidentate substituents. A generic p-block molecule AX_n will relax to its VSEPR-predicted shape if the *n* X substituents are capable of free motion along the surface of A (Figure 1a). Remotely tethering the X groups to one another outside the first coordination sphere of A restricts their motion in the vicinity of A, resulting in a ligand enforced geometric outcome that may be VSEPR non-compliant, depending upon the rigidity of the tether employed (Figure 1b). A large library of multidentate ligands have been developed in coordination chemistry studies on d- and f-block elements and, in principle, all of these may be co-opted or modified for use in p-block compounds.[20] Another strategy, which is relatively less common, is to use substituents that are sufficiently bulky that they dramatically widen the bond angles around the central element by steric repulsion (Figure 1c). The development of increasingly large substituents for providing kinetic protection of reactive sites has contributed significantly to this approach.[21-24] Finally, electron-donation can also stabilize non-classical geometries by partial occupation of any low-lying vacant orbitals that are exposed upon distortion (Figure 1d). This strategy can be used to access VSEPR-compliant molecules that exist in resonance or equilibrium with their "masked" VSEPR non-compliant forms.

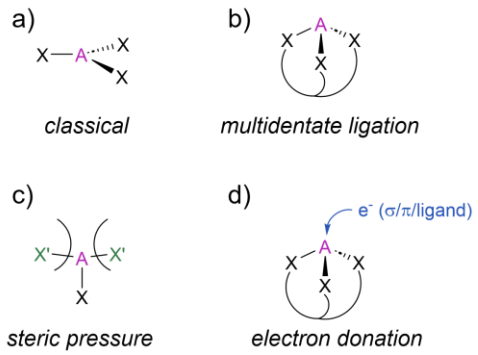

Figure 1. a) A VSEPR-compliant group 13 compound. b) Multidentate ligation, c) steric bulk, and d) electron-donation strategies to accessing VSEPR non-compliant geometries as applied to a group 13 compound.

The aim of this review is to provide an account of p-block molecular systems where ligands or substituents enforce a non-VSEPR geometric outcome using the strategies described above. It should be emphasized that in all cases more than one strategy is simultaneously operative: for example, multidentate ligands can also be sterically bulky, and it is impossible to avoid intramolecular electron donation from filled orbitals to vacant ones generated in a deformed molecule. Nevertheless, the classification has pedagogical value despite overlap. Also for pedagogical reasons, we use the conceptual framework of Walsh analysis to interpret the influence of the geometric distortion on a molecule's properties and reactivity. We focus on elements from Groups 13-16 and molecules that contain at least three electron pairs (bonding or non-bonding) at a central element. For practical reasons, we largely limit our discussion to non-hypervalent structures and those involving covalent rather than dative bonding, except when the dative bonding is used to transiently stabilize a non-VSEPR structure as in Figure 1d. Multinuclear compounds (e.g. congeners of alkenes or alkynes) or cluster compounds (e.g. pyramidanes) are also not considered here due to their extensive coverage elsewhere. [22, 25, 26] For a more comprehensive understanding of this field, the interested reader is also referred to related reviews focusing on pnictogen elements,[27, 28] applications in catalysis,[29] and multidentate ligands.[20, 30, 31] An earlier review by Bourissou and a recent book chapter by Greb are recommended as particularly valuable starting point.[32, 33]

Compounds with a Group 13 Central Element

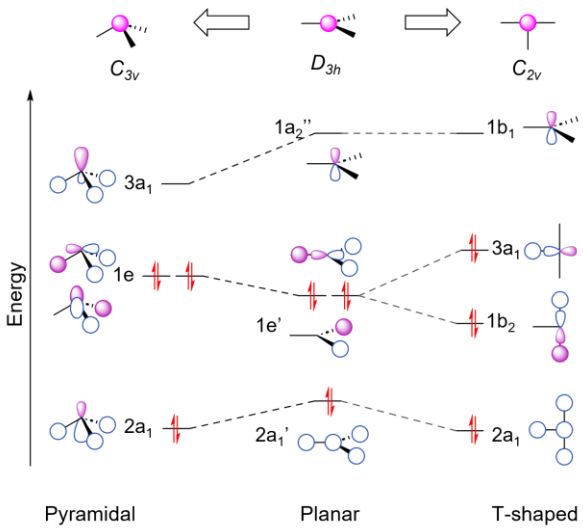

Figure 2. Qualitative Walsh analysis for deformation away from the VSEPR-consistent planar geometry of trivalent group 13 compounds.[34]

The VSEPR-geometry for Group 13 elements in the ground state is trigonal planar (D_{3h}), which leaves a vacant p-orbital available as the LUMO for coordination chemistry. As a result, the chemistry of the triels in the +3 oxidation state is dominated by Lewis acid behaviour. Ligand-enforced deviations from planarity towards either pyramidal and T-shaped geometries have been reported and these are expected to have different consequences for Lewis acidity, as described below.

Pyramidalization brings the Group 13 element into a geometry that is required to accommodate a Lewis base. Thus, computational studies have shown that the effect of ligand-enforced pre-pyramidalization is to favour the overall thermodynamics of Lewis acid-base formation, by reducing the distortion energy penalty incurred in the reaction.[35, 36] The LUMO ($1a_2''$ in D_{3h}) at the central element is also lowered in energy upon pyramidalization ($3a_1$ in C_{3V}) to give a frontier MO situation that is more conducive to coordination. In contrast, the D_{3h} to C_{2v} transformation maintains the molecular mirror plane. As such there is no major reduction in the coordination thermodynamics, nor an effect on the energy of the out-of-plane p(z) LUMO at the group 13 centre. Instead, the degenerate 1e'' HOMO of the D_{3h} molecule is split into a lowered

$1b_2$ MO and raised $3a_1$ HOMO from which it can be predicted that T-shaped molecules should exhibit greater nucleophilicity from their peripheral atoms. In terms of effect on the central group 13 atom, the distortion to C_{2V} alters the steric profile, making one hemisphere more available for reactivity.

Boron compounds:

The remarkably simple compound 1-boraadamantane, **1**, first reported in 1973 by Mikhailov,[37] remains the only example of a persistent, isolable, and significantly-pyramidal borane (Figure 3a). The initial synthesis has been much improved,[38] enabling detailed reactivity studies summarized elsewhere.[39, 40] The solid-state structure of this compound remains unknown due to high degree of orientational disorder, which is also borne out from its low frequency Raman spectrum that showed lattice vibrations as broad ill-defined peaks.[41] Interestingly, the Raman spectrum did show a highly crystalline phase below 183K, but an X-ray analysis of this phase has not yet been reported. Meanwhile, the structure of 3-methyl-1-boraadamantane has been studied by Mitzel using gas-phase electron diffraction (GED), confirming the slight pyramidalization at boron (ΣC-B-C = 349.4(4)° vs 360.0° in BMe_3).[42] The B-C bonds were found to be slightly shorter than expected (1.561(10) Å in 3-methyl-1-boraadamantane vs 1.578(1) Å in GED of BMe_3[43]), and C-C bonds adjacent to B found to be longer (1.589(7) Å) than elsewhere in the cage (1.543(8) Å). Together with NMR experiments on **1** reporting smaller than expected $^1J_{C\text{-}C}$ coupling constants for bonds adjacent to boron,[44] these observations support the notion of C-C to B(pz) hyperconjugation that stabilizes the pyramidal form by partial occupation of the vacant p(z) orbital (Figure 3b). The extent of stabilization has been estimated by NBO calculations to be ca. 15 kcal/mol, indicating a major perturbation of the electronic structure.[42] Note that such interactions are well-known in the iso-electronic adamantyl cation, resulting in flattening of the CC_3 pyramid.[45] They have also been computationally predicted for Si-C bonds adjacent to a vacant B(2p) centre.[46] Despite hyperconjugative stabilization, **1** shows clear evidence of enhanced Lewis acidity relative to comparable planar boranes. For example, its pyridine adduct does not dissociate even at 200 °C,[39] and it shows a higher calculated binding affinity for pyridine (116 kJ/mol) than does planar triethylborane (86 kJ/mol).[47]

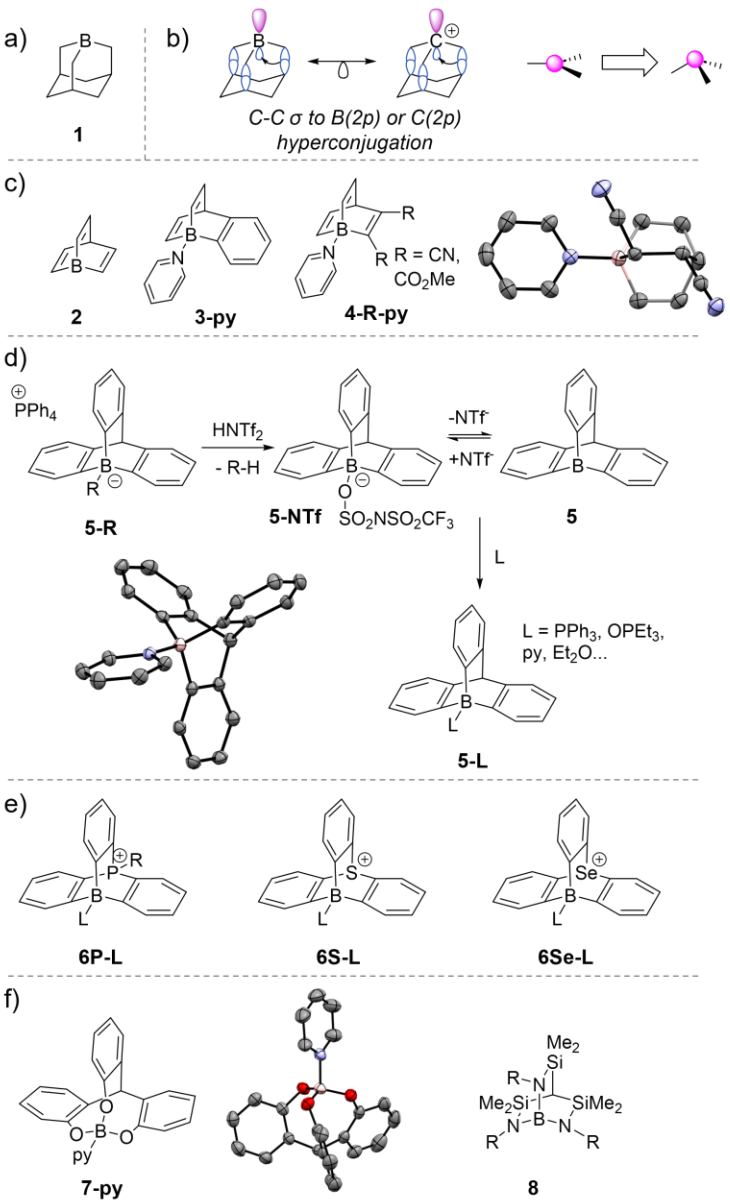

Figure 3. Pyramidalized borane compounds. Selected solid state structures (CCDC # 607628, 1986934, 288842) are also shown with hydrogen atoms omitted and ellipsoids set at the 50% probability level. NTf = $N(SO_2CF_3)_2$.

Related borane cages derived from 1-borabarrelene were reported by Piers in Lewis base stabilized form (Figure 3c) via the Diels-Alder cycloaddition of 1-borabezenene with either alkynes or benzyne.[48] The degree of pyramidalization at boron in pyridine coordinated 1-borabarrelenes (**2-py** and **3-R-py**, ΣC-B-C = ca. 312°) is significantly greater than in other pyridine-borane adducts (e.g. those with triarylboranes show ΣC-B-C = ca. 330°), reflecting the structural constraints of the

barrelene cage. The high extent of pyramidalization portends a very high boron-centered Lewis acidity, which is confirmed by the observation that the B-N bond lengths in **2-py** and **3-R-py** are shorter than the corresponding values in other pyridine-borane adducts. Moreover, NMR studies found no evidence of Lewis base dissociation from **2-py** and **3-R-py** adducts even at 200 °C in solutions of d_5-pyridine, and thermogravimetric analysis showed extrusion of alkynes (retro Diels-Alder involving C-C bond fission) was more favourable than pyridine dissociation. In line with these observations, DFT calculations show that the pyridine binding affinity of 1-borabarrelene (176 kJ/mol) greatly surpasses the value for triethylborane (86 kJ/mol) or BPh_3 (79 kJ/mol).[47]

The 1-boratriptycene framework (**5**) is a close analogue of 1-borabarrelene but features aromatic flanking groups, which further constrain and rigidify the molecule. Berionni showed that **5** could be transiently accessed by in-situ dearylation of triptycene arylboronate anions (**5-R**) by strong Bronsted acid $HNTf_2$ (Figure 3d).[47] Addition of Lewis bases in a subsequent step yielded the base-stabilized 1-boratriptycenes (**5-L**). ^{11}BNMR assays after adding $HNTf_2$ but before adding the Lewis base showed a broad resonance at intermediate values between the computed value for base-free **5** (90 ppm) and the starting materials (-12 ppm), indicating a dynamic equilibrium between **5** and its NTf_2 coordinated form **5-NTf**. The two-step protocol enabled access to several Lewis base adducts. Notably, thermogravimetric analysis of the Et_2O adduct, **5-Et_2O** revealed loss of the Lewis base at 175 °C, but the analogous experiment with the pyridine adduct featured a more complex, multi-step, decomposition process. In terms of Lewis acidity, **5** shows a calculated pyridine affinity (200 kJ/mol) and fluoride ion affinity (476 kJ/mol) that is exceptional for neutral boranes, and comparable to values of heavily fluorinated derivatives like $B(C_6F_5)_3$ (pyridine affinity: 144 kJ/mol, fluoride ion affinity: 466 kJ/mol).[47] While structural data are unavailable for free **5**, the calculated structure shows a much greater degree of pyramidalization (ΣC-B-C = ca. 339°)[47] compared to derivatives of **1** (349.4(4)° for 3-methyl-1-boraadamantane), which is consistent with the high observed electron pair accepting ability.

While these pyramidal borane cages clearly exhibit enhanced Lewis acidity due to their structural deformation, the extent to which hyperconjugative effects involving C-C σ bond to B(pz) overlap (as noted for **1**) modulates the LUMO energies has not been comprehensively studied. However, the effect of conjugation between two *vacant* σ-type orbitals and that of molecular

charge on boosting the Lewis acidity of pyramidal boranes has been explored. Berionni reported the dearylation of zwitterionic triptycene-like phosphonium boronates to isolate base-stabilized cationic 9-bora-phosphatriptycenes (**6P-L**, Figure 3e).[49] Calculations revealed that the base free borane, **6P**, features one of the most Lewis acidic trivalent boron centres known. In these compounds, the cage topology enforces overlap between the phosphonium σ* antibonding orbital and the B(pz) orbital. Together with the Coulombic effect of the positive charge, and the pre-pyramidalization at boron, calculated fluoride ion affinities exceeding 800 kJ/mol are observed, comparable to those of uncoordinated silylium cations. The analogous base-stabilized cationic 9-bora-thiotriptycene and 9-bora-selenotriptycenes have also been reported recently (**6S-L** and **6Se-L**).[50, 51] The larger backbone atom in these cages allows for slight structural relaxation reducing the degree of pyramidalization at boron. Nevertheless, such cations exhibit very high Lewis acidity, which was harnessed for challenging C-H activations as well as a very rare case of C(sp3)-Si bond cleavage.[50]

A more flexible boratriptycene framework can be formed using tris-phenolate ligands, as reported by Yasuda and Baba in base stabilized form **7py** (Figure 3f).[52] In this case, the larger central cage enables the boron centre to be nearly planar (calculated 359.7° for base-free **7**), but the caged borates are nevertheless significantly more Lewis acidic than uncaged ones. For example, the calculated pyridine-binding affinities of $B(OPh)_3$ and base-free **7** are 52 kJ/mol and 80 kJ/mol, respectively. This enhancement within the cage environment is a result of the oxygen lone pairs being unable to twist into the ideal orientation for overlap with the vacant B(2p) orbital. By comparison, B-O bond free rotation in uncaged borates sike $B(OPh)_3$ readily permits such twisting. The reduction in O(n)→B(2p) conjugation illustrates another mechanism by which geometry enforcing ligands can perturb electronic structure at the central element, without formally distorting it away from its VSEPR-predicted minimum geometry. The Chen group reported a related triamino borane derivative **8**, for which similar structural and electronic considerations are operative.[53] The sum of angles around boron in this case is only marginally smaller (355.7°), but nevertheless illustrative of a slight deviation from the VSEPR trigonal planar geometry.

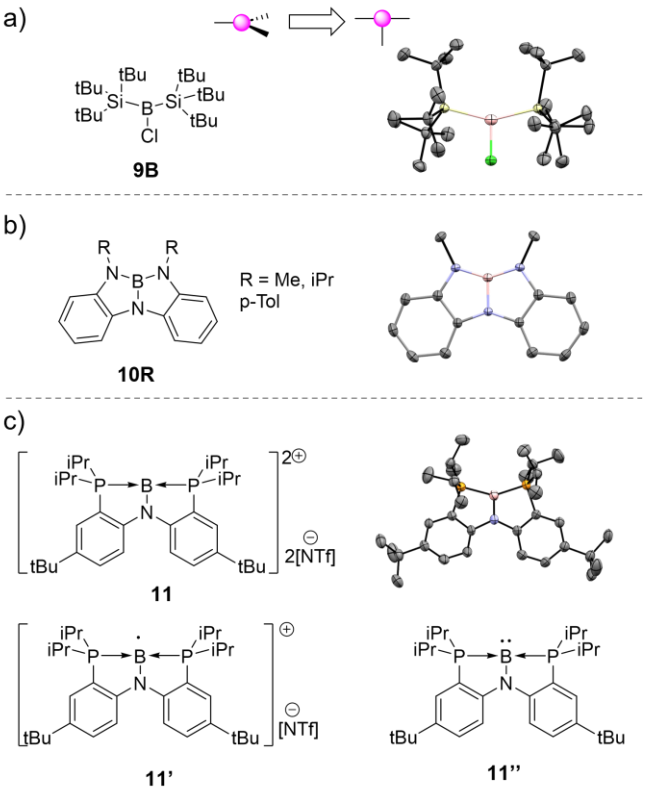

Figure 4. Approximately T-shaped boranes. Selected solid state structures (CCDC # 163513, 1547725, 2269947) are also shown with hydrogen atoms omitted and ellipsoids set at the 50% probability level. NTf = $N(SO_2CF_3)_2$.

Braunschweig has reported several examples of T-shaped boranes that feature transition metal-boron multiple bonding.[54] The geometries of these complexes are difficult to classify as being 'ligand-enforced', but rather reflect the unusual and interesting electronic structure enabled by the Z-type coordination. Wiberg reported bulky bis-silylated chloroborane (**9B**, Figure 4a), where the extreme steric clash between the Si^tBu_3 groups provides sufficient driving force to widen the Si-B-Si angle to ca. 152°, without requiring any ligand tethering.[55] The nucleophilicity of the remaining halide is expected to be high due to the raised HOMO in such T-shaped compounds, but reactivity studies have not been reported. Martin reported on the use of an NNN pincer framework to make T-shaped boranes with N-B-N angles in the 144.9(2)-146.0(2)° range (**10R**, Figure 4b).[56] The electronic structure of these compounds showed extensive conjugation over the planar 6-5-5-6 fused ring containing 18 π-electrons. Indeed, their LUMO is a π*

antibonding MO that is primarily ligand based, whereas the LUMO + 2 shows some B(2p) contribution mixed in with other ligand-centric MOs. The excellent N-B π-overlap is expected to attenuate the Lewis acidity at the boron centre, although this feature was not explored. More recently, Su and Kong used a monoanionic PNP pincer ligand to access boron centres within a T-shaped environment (**11**, **11'**, and **11''**, Figure 4c.).[57] The replacement of two anionic N groups (in the NNN ligand) with two phosphine arms reduces the π-donation into the B(2p) and enables the introduction of sequential cationic charge. The P-B-P angles observed at the tetrahedral centres vary in the 125.7(2)-131.9(2)° range (109.5° expected for unconstrained tetrahedron), while those at the T-shaped centres vary in the 141.0(3)-146.4(2)° range (120° expected for unconstrained trigonal planar). One of the most interesting aspects of the observed structures is the relative similarity spanning three charge states, illustrating the PNP ligand as a robust platform for stabilizing a wide range of electronic environments. As expected, the polycations exhibit very high Lewis acidity (exceeding that of SbF_5 towards fluoride), while the neutral species exhibits boron-centred nucleophilicity.

Aluminum and Gallium Compounds: The use of ligand-enforcement to achieve non-VSEPR geometries is less developed for the heavier group 13 elements. Whereas **1** has been known for nearly half a century, 1-alumaadamantane or heavier analogues remain unknown, although computational studies predict them to also exhibit high Lewis acidity.[35, 36] Extending the strategy used to isolate pyramidal boranes, Fukase, Konishi, and Yasuda reported pyridine stabilized caged alane **12Al-py** (Figure 5a) which features electron-withdrawing bromine substituents in the ortho positions of the aryl arms.[58] This compound proved to be a potent Lewis acid catalyst for stereoselective glycosylation, although the mechanism involved an increase in the coordination number at aluminum to five rather than dissociation of the pyridine ligand to reveal base-free, three-coordinate **12Al**. Wiberg reported approximately T-shaped chloroalane, $(tBu_3Si)_2AlCl$ (**9Al**), and halogallane $(tBu_3Si)_2GaCl$ (**9Ga**) derivatives of the previously mentioned **9B** using bulky silyl groups that result in a Si-M-Si angle of 148.25(2)° and 152.94(1)°, respectively. Attempts to isolate the aluminum analogues of T-shaped boranes by use of trianionic NNN or ONO ligands were frustrated by formation of complex aggregates.[59] Notably, a dianionic dialane (**13**, Figure 5b) featuring heavily distorted aluminum centres could be accessed by Su and Wang during these

studies.[60] In contrast to the ethane-like structure of reported dianionic dialanes, the hemispheric constraint of the NNN ligand results the formation of an AlN_3 semi-pyramid at each end of the Al-Al bond. The anion also exhibits more exposed metal centres, with potential consequences for coordination chemistry that remain to be explored.

Distortion of four-coordinate aluminum or gallium centres from their classical tetrahedral geometries to planar ones has been reported using multidentate ligands. Berben used a dianionic imino-diamido ligand to access neutral, square planar complexes **14Al** and **14Ga**, for which extensive delocalization and aromaticity was established using careful ^{1}H NMR spectroscopic analysis and found to be critical in enforcing the square planar geometry (Figure 5c).[61, 62] Despite partial population of the p-orbital at the metal in such complexes, it was possible to form square pyramidal Lewis base adducts (e.g. **15**), illustrating residual electrophilicity that could be harnessed for challenging bond activation and dehydrogenative coupling.[63] Riddlestone reported an analogous dianionic pincer complex of aluminum (Figure 5c) that showed CO_2 insertion into the Al-N bond due to the high metal centred Lewis acidity.[64] This reactivity was coupled with reduction to achieve the net catalytic hydroboration of CO_2.

Anionic triels are also classically tetrahedral molecules. Greb used calix[4]pyrrolate ligands to prepare salts of anions [**17Al**]$^-$ and [**17Ga**]$^-$ (Figure 5c) showing unusually high Lewis acidity for anionic species. [65, 66] The origins of the high Lewis acidity have been thoroughly-discussed with referenced to Walsh analysis elsewhere, and are therefore not reproduced here.[67] Highlighting consequences for reactivity, the adjacency of a low-lying vacant p-orbital and heteroatoms or other electron-dense components of an anionic ligand unlocks metal-ligand cooperativity that can be harnessed for catalytic reactivity (Figure 5d) such as dehydropolymerization of phosphine-boranes.[65, 68, 69]

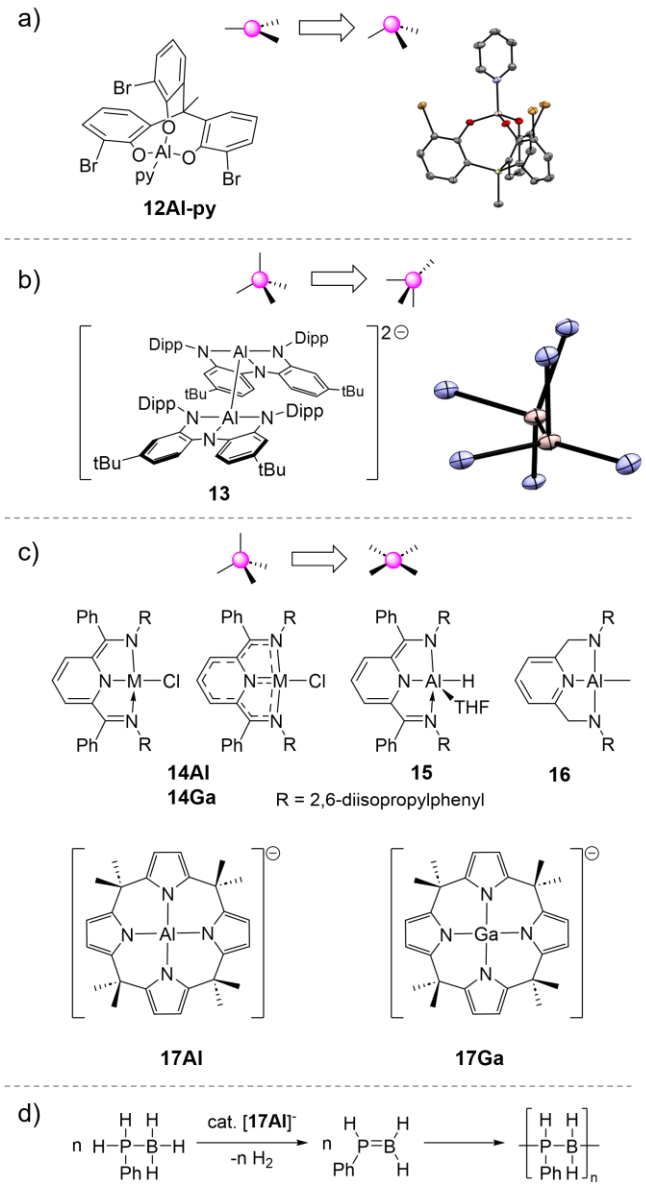

Figure 5. a) Pyramidalization of a trivalent alane. b) An NNN pincer supported dialane dianion **13**. Portion of the solid-state structure of the dianion emphasizing arrangement of the Al_2N_6 moiety. Hydrogen atoms omitted and ellipsoids set at the 50% probability level. c) Distortion at four-coordinate aluminum centres. d) Catalytic dehydrogenative coupling of phosphine boranes by a square planar aluminum anion.

Compounds with a Group 14 Central Element

Four-coordinate carbon compounds were long believed to only exist in the tetrahedral geometry, as first proposed in 1874 by van't Hoff and Le Bel.[70, 71] Since then, several carbon centres featuring unusual geometries have been considered,[72-76] initially as transition state models,[77] and later experimentally by stabilization using transition metals[78] or highly strained cyclic systems.[79] An extensive discussion of these compounds falls outside the scope of this review, and this section will instead focus on the heavier analogues of carbon. Despite early calculations showing the lower energy barrier required for the planarization of four-coordinate silicon species compared to carbon, experimental realization of planarization for the heavier group 14 elements has only occurred recently.[67, 80-101]

When considering unusual geometries in group 14 compounds, it is instructive to consider the inversion pathways for tetrahedral molecules. The inversion of methane has been extensively investigated computationally,[102-104] finding that it occurs not through a planar D_{4h} transition state but rather a distorted C_s transition state (Figure 6).[105] The square planar inversion of heavier tetrahedral p-block compounds was more recently investigated computationally, finding low barriers for a number of these compounds.[67, 88] While square planar inversion is not the most favorable pathway for most of the element hydrides,[88] depending on the substituents the planar transition state can be significantly stabilized.[67] This allows some insight into how a planar group 14 compound can be stabilized on an electronic basis. Two key factors of the substituents were identified as lowering this inversion barrier and thus making the transition state more accessible: i) a σ-acceptor effect where more electronegative substituents lower the inversion barrier, and ii) a π-donor effect where π-donating substituents lower the inversion barrier.[67] These electronic effects are key to stabilize a non-VSEPR group 14 complex in addition to the geometric constraining ligands.

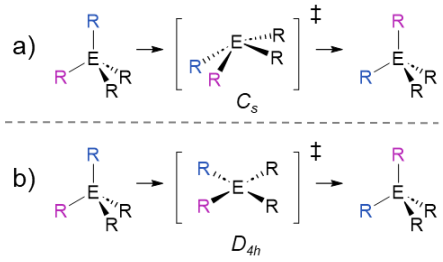

Figure 6. Two possible inversion pathways for tetrahedral compounds. a) Inversion via a C_s transition state as found for CH_4; b) Square planar inversion via D_{4h} transition state.[67]

A qualitative Walsh diagram looking at the orbital picture of SiH_4 in the tetrahedral and square planar geometry is shown in Figure 7.[67] This analysis demonstrates why the tetrahedral geometry is favored electronically: the tetrahedral arrangement shows four sets of bonding and antibonding orbitals, while in the square planar case one of these filled orbitals is now non-bonding. The significant destabilization of one of the degenerate $1t_2$ orbitals upon planarization is not offset by the slight stabilization afforded to the other two $1t_2$ orbitals resulting in the square planar configuration being higher in energy and thus unfavorable.[67] However, this Walsh diagram also reveals the unique properties geometric deformation can afford to group 14 centres through planarization. Due to the destabilization of one filled orbital (b_{1g}) and the stabilization of one empty orbital (a_{2u}) when going from tetrahedral to square planar, a decrease in the HOMO-LUMO gap is expected, which should enable unique reactivity. Moreover, a vacant p-orbital is generated as the LUMO at the central element, with accompanying predictions of Lewis acidity.

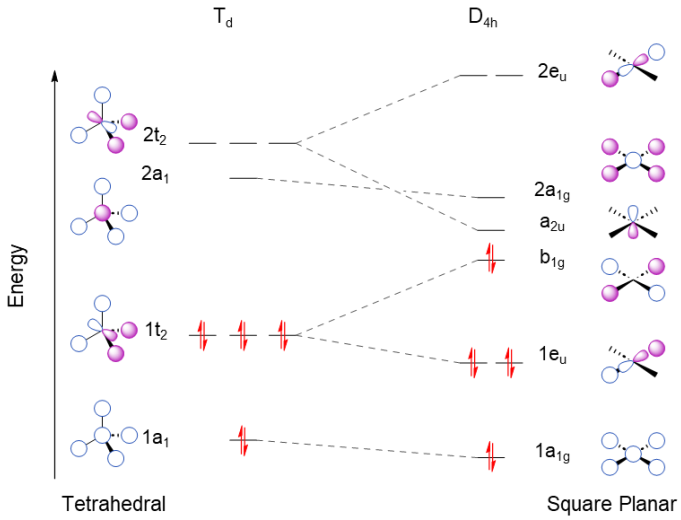

Figure 7. Walsh diagram for the distortion of SiH_4 from tetrahedral to square planar.

Silicon

The first claim of a planar four-coordinate silicon compound appeared in 1979, with the synthesis of bis(*o*-phenylenedioxy)silane **18** (known since 1951)[106] and comparison with the tetrahedral carbon analogue.[107, 108] However, due to the lack of complete crystallographic evidence for the planar structure of this compound, this report has been the focus of considerable debate.[109] More recent investigations on this system have confirmed that **18** is monomeric only in a neon matrix in which it is tetrahedral at silicon, otherwise this compound is prone to oligomerization.[110] Other early attempts at the planarization of four-coordinate silicon took inspiration from the carbon systems of strained rings. One notable example is the synthesis of a tetraazasilafenestrane **19**, which features distorted N-Si-N angles between 92° and 122°.[111] While this compound is clearly not planar, it does show substantial deformation from the standard tetrahedral geometry at four-coordinate silicon. The multidentate nature of the ligand is a key enabling feature, as related compounds such as the silatetraazaspiroalkane, **20**, are tetrahedral with respect to the SiN_4 core.[112] While the π-donating nature of the nitrogens does have an effect on lowering the energy required for planarization at silicon,[80, 111] it is clear that the rigidity of this ligand is as important as the electron donation considerations.

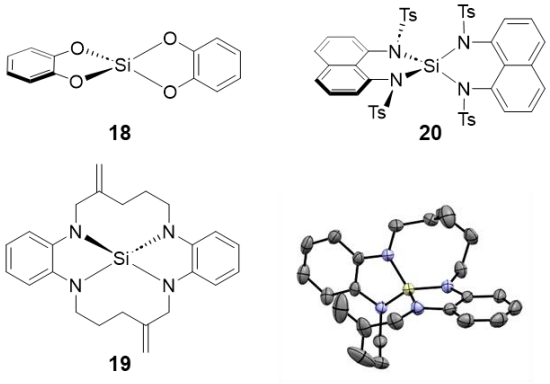

Figure 8. Some four-coordinate silicon compounds showing the geometry at silicon. Compounds **18** and **20** are tetrahedral, while **19** is slightly distorted as seen in the molecular structure: CCDC # 102562. Hydrogen atoms omitted and ellipsoids set at the 50% probability level.

More recent geometrically deformed silicon complexes are based on a tridentate pincer ligand framework. Utilizing an ONO ligand framework dimeric silicon species **21** were accessed with a variety of different substituents on silicon.[113] While this silicon center is five-coordinate and not planar, it can be conceived as a dimer of two distorted silicon species, providing some insight into the use of pincer ligands to deform the geometry at silicon. Related silicon compounds **22** and **23** featuring NNN and ONO tridentate ligands have also been accessed which exist as either monomers or dimers depending on the steric bulk of the fourth substituent at silicon.[114] The monomeric compounds show a large deviation from standard tetrahedral bond angles (**22**: N1-Si-C1 = 126.17°, N2-Si-N3 = 129.67°; **23**: N1-Si-C = 128.35°, O1-Si-O2 = 121.07°) but are still not fully planar.[114] As a tridentate ligand is used the fourth substituent is not tethered and is able to point out of plane, while the ligand framework shows some bending (Figure 9). The increased rigidity of this ligand imparted by the phenyl backbone and additional steric bulk enabled greater deformation at silicon for **22** and **23** compared with **21**. However, as silicon is four-coordinate a tridentate ligand in which the fourth substituent is not subject to any geometric constraint is insufficient to access a fully planar, four-coordinated silicon compound.

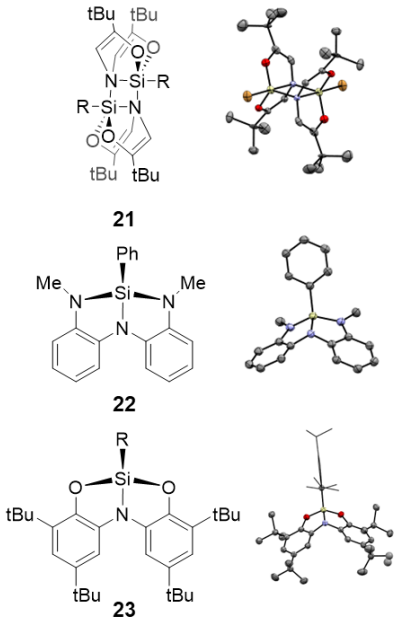

Figure 9. Distorted silicon compounds supported by tridentate pincer ligands. Molecular structures shown to illustrate deviation from tetrahedral geometry; **21**: CCDC # 274140, **22**:

CCDC # 1565853, **23**: CCDC # 1566286. Hydrogen atoms omitted and ellipsoids set at the 50% probability level.

The first report of a truly planar, four-coordinate silicon species appeared in 2000 with the report of the $SiAl_4$ anion in the gas phase.[115] As this molecule was detected in the gas phase and not isolable, the structure was not confirmed by X-ray crystallography and instead the planar structure is supported by computational investigations.[115] The germanium analogue of this was also accessible via the same route and detected in the gas phase.[115] In the last few years a number of four-coordinate planar silicon compounds have been reported which are isolable and confirmed to be planar by X-ray crystallography. Each of these compounds feature a unique bonding environment with different methods of stabilizing the planar silicon center which will be discussed here.

Iwamoto reported planar silicon compound **24**, which features a planar tetrasilane core with a unique single π bond (but no underlying σ-bond) between two of the silicon atoms.[116] Two crystalline forms of this compound were observed, one with a fully planar structure and one which features a slight bending of this core. The slightly bent structure was determined to be the structure in solution based on computational investigations and the silicon NMR chemical shift observed.[116] The unique nearly planar environment about the bridgehead silicon atoms is attributed to the large steric bulk around the tetrasilicon core.[116] Another strategy for accessing planar silicon compounds is through the use of transition metals to stabilize the silicon core as evident in compounds **25** and **26**, reported by Filippou.[117] These trapezoidal silicon centres are stabilized by coordination with either molybdenum or tungsten in homobimetallic complexes. The electronic structure of these complexes were comprehensively analyzed using computational techniques to help explain the stabilization of the planar silicon centre. An interesting factor which stabilizes the planar silicon centre in addition to the transition metal interactions is aromaticity within the central SiC_2 ring due to two delocalized π electrons.

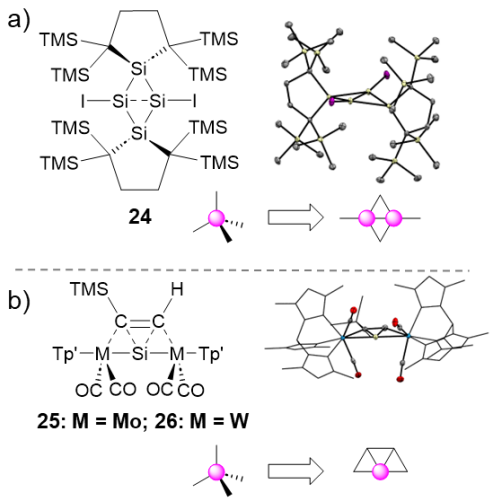

Figure 10. a) Planar four-coordinate silicon compound with a 'butterfly' type structure **24**: CCDC # 1992432. b) Planar silicon compounds supported by transition metals **26**: CCDC # 2035117. Hydrogen atoms omitted and ellipsoids set at the 50% probability level.

The use of a rigid, tetradentate ligand is another strategy which has been utilized to access planar silicon compounds. One example is the use of the rigid macrocyclic calix[4]pyrrole ligand[31] in silicon chemistry, as shown by Greb.[118, 119] An extremely stable five-coordinate anionic hydrosilicate **27** was accessed in this framework which surprisingly does not act as a hydride donor in contrast to other hydrosilicates.[118] The high stability of this compound was attributed to the planar silicon core showing a high hydride affinity by computational measures due to the low energy LUMO which corresponds to a vacant p_z orbital at silicon.[118] The neutral, four-coordinate, planar silicon complex **28** was also able to be accessed utilizing this calix[4]pyrrole ligand.[119] This complex displays a dramatically reduced LUMO energy and HOMO-LUMO gap compared to tetrahedral silicon(IV) species.[119] Compound **28** was able to participate in ligand cooperative reactivity (analogous to aluminates and gallates in this ligand framework), activating the C-C triple bond of phenylacetylene in a 1,2-addition to give **30**.[119] This reactivity is unprecedented for silicon(IV), demonstrating the powerful effects of ligand enforced geometric deformation on main group compounds.

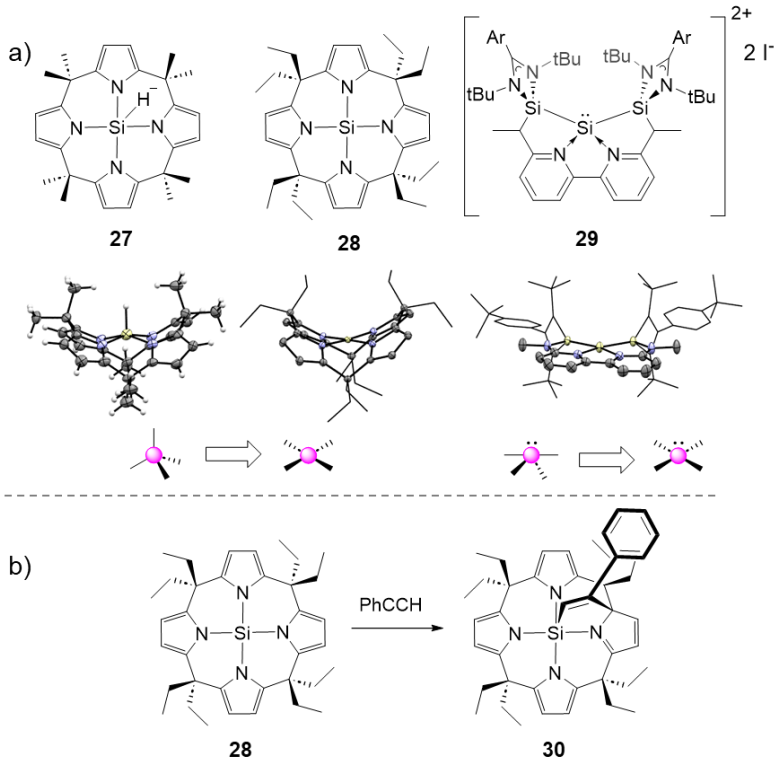

Figure 11. a) Square planar silicon complexes and their molecular structures to show planarity of silicon centre along with diagram showing change in geometry. **27**: CCDC # 2042941, **28**: CCDC # 1879804, **29**: CCDC # 2226326. Hydrogen atoms omitted and ellipsoids set at the 50% probability level. b) Reaction of compound **28** with phenylacetylene to give **30**.

Another example utilizing a rigid tetradentate ligand to access planar silicon species is Driess' planar silicon(II) complex **29** supported by a bis(*N*-heterocyclic silylene) bipyridine ligand.[120] While not strictly within this review's scope due to the planarity being a result of additional coordination, it is noteworthy that this species shows not only planarity but also a very wide angle between the amidinate groups of approximately 111 °. This dication features a planar central silicon atom with a lone pair of electrons localized in the silicon p_z orbital, in contrast to most silylenes in which the lone pair is localized in an s orbital.[120] The compound is reversibly interconverted with a hexacoordinate silicon(IV) species by reaction with I_2 and a reduction to return to **29**.[120]

Another strategy which has been used to access geometrically distorted silicon compounds is the use of steric bulk. The use of particularly bulky substituents on silicon results

in dramatically widened bond angles compared to those predicted by VSEPR (some examples shown in Figure 12). One example is Sekiguchi and Akiyama's report of a triplet silylene **31** featuring two extremely bulky $SitBu_3$ substituents which force this compound to have a wide angle about the silicon centre due to steric repulsion.[121] While a crystal structure for this compound was not obtained to determine the exact bond angle, for the silylene to be in the triplet state (as confirmed by EPR spectroscopy), a Si-Si-Si bond angle of at least 120 ° is required. Reactivity studies confirmed that the geometric perturbation has a pronounced effect on not only spectroscopic properties, but also reactivity for this molecule, which shows addition to rapid intramolecular C-H activation upon being generated. A related example is **32** which once again has two very bulky $SitBu_3$ groups but in this case the central silicon is four-coordinate with two chloride substituents.[122] The structure of this compound was confirmed crystallographically, finding a very wide Si-Si-Si bond angle of ca. 143 ° due to the steric bulk of the substituents. The largest reported Si-Si-Si bond angle was found in **33**, with the silylene radical cation supported by an N-heterocyclic carbene featuring an angle of ca. 145 °.[123] A related silylene **34** was also accessed which features a wide N-Si-N angle enforced by both large steric bulk and the use of ferrocene as a geometrically constraining framework.[124] Similar stannylenes and plumbenes featuring wide angles have also been accessed using this strategy.[125, 126]

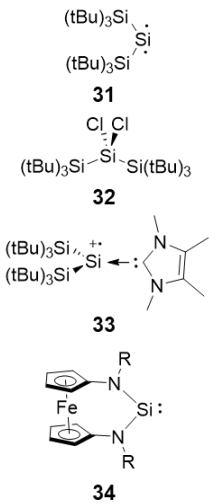

Figure 12. Silicon species featuring wide angles at silicon due to steric bulk or ligand constraint.

Germanium, Tin, and Lead

While the synthesis of planarized complexes of the heavier group 14 elements has been less common than for carbon or silicon, there are still a few examples, particularly for germanium and tin. The use of a tridentate ONO ligand as in the previously discussed **21** was also applied to the heavier group 14 elements. Dimers of germanium and tin, **35** and **36**, featuring a significant distortion from tetrahedral geometry were able to be accessed, however the same could not be accomplished for lead.[127] Using germanium or tin (II) sources enables access to these distorted dimers in the +2 oxidation state, while the use of a germanium (IV) starting material gave a six-coordinate germanium (IV) complex.[127]

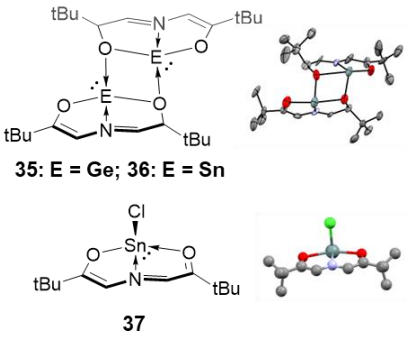

Figure 13. Heavier group 14 non-tetrahedral, four-coordinate complexes supported by tridentate pincer ligands and their molecular structures **36**: CCDC # 237517, **37**: CCDC # 1162424; **37** is shown in the ball and stick model due to unavailability of full data. Hydrogen atoms omitted and ellipsoids set at the 50% probability level.

An early report of a distorted four-coordinate tin species utilizes this same ONO pincer ligand to access a hypervalent tin center with 10 valence electrons, **37**.[128] Due to the redox active nature of the ligand this complex features a formally Sn(II) centre with the observed geometry in which the chloride points straight down due to the lone pair present. This Sn(II) character is realized experimentally as the tin can be oxidized using SO_2Cl_2 to give a six-coordinate complex.[128] A very similar distorted four-coordinate Sn(II) complex was able to be accessed utilizing a rigid PNP pincer ligand.[129] As there are lone pairs in the germanium and tin centres discussed here, the geometry does not experience a significant distortion from that expected by VSEPR theory. In this way the geometry observed in compounds **35-37** is not considered to be a ligand enforced, but

rather the expected geometry for four-coordinate Ge/Sn(II) compounds which are supported by pincer ligands. A number of similar low-valent (0 or +1) germanium and tin complexes have been accessed through the use of pincer ligands.[130-134] In these complexes the metal centres feature either one lone pair and a metal-metal bond, or two lone pairs and thus do not deviate from their VSEPR predicted geometry.

More recently, some examples of ligand enforced geometry at heavier group 14 element centres have been accessed where the geometry differs from the VSEPR predicted minimum due to the ligand used. A nearly planar Sn(II) species was reported by Greb using the rigid calix[4]pyrrole four-coordinate ligand to give the dianionic species **38**.[135] While not planar, this tin center displays significant distortion from the VSEPR predicted geometry by possessing a square-pyramidal geometry. Due to the lone pair at the Sn(II) centre, **38** acts as a σ-donating ligand in coordination with transition metals.[135] This complex is able to react as a nucleophile with a variety of C-Cl bonds resulting in a five coordinate tin center and the loss of a chloride. Additionally, **38** acts as a two electron reductant, converting iodobenzene into benzene with the concurrent oxidation to a Sn(IV) compound.[135] Recently, Wang and Su reported a planar T-shaped germanium anion **39** using a rigid NNN tridentate ligand.[136] This metal centre is fully planar, and only three coordinate allowing for the tridentate ligand to support this planarization. The rigid, tridentate nature of this ligand enables the observed T-shaped geometry of **39**, as a trigonal pyramidal geometry would be expected in the unconstrained case. Complex **39** does not react with nucleophiles due to partial occupancy of its 3p SOMO (and the negative charge), but readily reacts with electrophilic methyl iodide to give a four-coordinate neutral germanium complex and can be oxidized by sulfur or selenium.[136]

Greb reported the synthesis of a calix[4]pyrrole complex of germanium, which was isolated as the bis-THF adduct **40**.[137] This complex is structurally similar to a previously reported germanium cation which was found to be extremely unstable.[138, 139] As the THF adduct this complex does not have a non-VSEPR geometry as it is octahedral, however, if the molecules of THF are considered to be labile then it can be envisioned as a 'masked' square planar germanium compound. The lability of the THF donors was experimentally confirmed in the reactivity of this compound which displays Lewis acidity with the ability to add various anions and abstract fluoride

anions from other Lewis acids.[137] This complex also displays ligand cooperative bond activations, ability to add OH bonds, activate carbonyls and even the CN triple bond in acetonitrile.[137] An example is highlighted in the ligand-cooperative activation of isopropanol by **40** to give **41** (Figure 14).

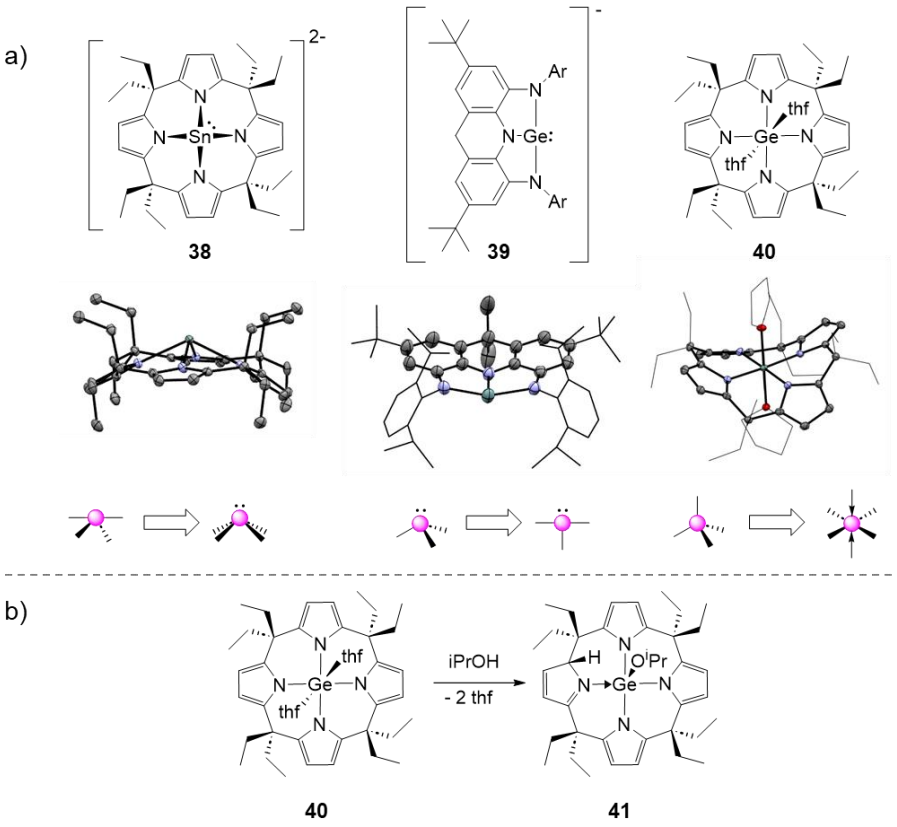

Figure 14. a) Heavier group 14 complexes which deviate from the expected VSEPR defined geometry and their molecular structures **38**: CCDC # 2125918, **39**: CCDC # 2121989, **40**: CCDC # 2259393. Hydrogen atoms omitted and ellipsoids set at the 50% probability level. b) Ligand-cooperative reactivity of **40** with isopropanol to give **41**.

Compounds with a Group 15 Central Element

Most reports on ligand enforced geometry changes in pnictogen compounds are based on sterically constrained bicyclic phosphines, a class of compounds which have been recently reviewed.[140] The most significant early report was by Arduengo and co-workers in 1984 reporting

the synthesis and properties of the T-shaped ONO coordinated phosphorus compound **42**.[141, 142] Early work on this and related systems were undertaken by a number of groups including those of Wolf, Baccolini, Contreras, and Schmidpeter.[143-150] In these early reports a key structural feature emerged in which the unsaturated backbone present in **42** is essential to stabilize this T-shaped geometry, while compound **43** as reported by Wolf and co-workers contains a saturated backbone and is not T-shaped.[142-144] This can be explained based on the resonance structure for **42** in which two lone pairs are present at phosphorus (Figure 15). The 10-P-3 (where 10 refers to the number of electrons at phosphorus and 3 refers to the coordination number) compound **42** enables this T-shaped geometry while the 8-P-3 configuration in compound **43** results in a bent structure that is closer to the VSEPR predicted geometry for phosphorus.[142] Despite these exciting early reports throughout the 1980's and 90's, interest in these non-VSEPR pnictogen compounds largely faded until the last 10 to 15 years.[142] Recent reports showing exciting reactivity and catalytic activity for these compounds have sparked considerable interest and will be discussed herein.[151] Other pnictogen compounds featuring unusual structural features such as planar phosphonium cations, pnictinidenes or Pn-Pn multiply bonded systems, and "bell-clapper" compounds fall outside of the scope of this review and will not be discussed here.[152-157]

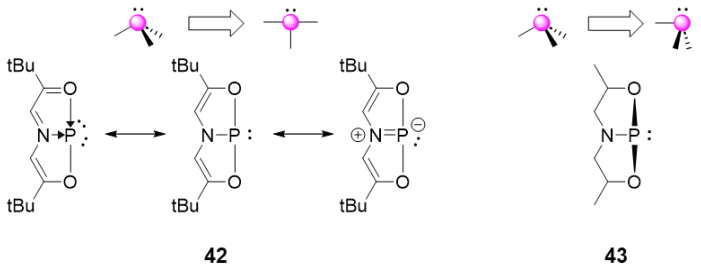

Figure 15. T-shaped phosphorus compound **42** with important resonance contributors and pyramidal phosphorus compound **43** and diagrams showing distortion of the phosphorus centre imparted by the ligand.

Inversion processes at trigonal pnictogen centres can provide some insight into the stabilization of planar distorted pnictogen compounds. The inversion processes of pnictogens have been comprehensively investigated and will only be discussed briefly here.[158, 159] The traditional vertex inversion process proceeds through a trigonal planar D_{3h} transition state (Figure

16). In the case of phosphines which are electron deficient a different inversion process is favored, edge inversion (Figure 16). The edge inversion process occurs via a T-shaped C_{2v} transition state, which is the same geometry as T-shaped compound **42**. In addition to this inversion process being favored by electron deficient phosphines, due to the geometry enforced by the pincer ligand, phosphines such as **43** also invert via this edge inversion process. To stabilize an isolable planar pnictogen, a pincer-type ligand is needed to lower the energy of the planar structure, just as it stabilizes the inversion transition state for non-planar pnictogens such as **43**.

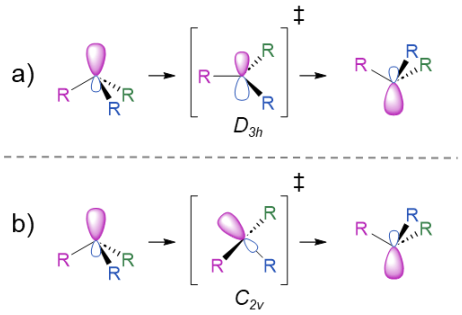

Figure 16. a) Vertex inversion of pnictogen centres via D_{3h} transition state. b) Edge inversion of pnictogen centres via C_{2v} transition state.

A qualitative Walsh diagram of the deformation from trigonal pyramidal to planar is shown in Figure 17. As many of the compounds discussed herein are not fully planar, deformation to both the C_{2v} and the C_s geometry is also considered. In the simplified frontier MO diagram for a typical trigonal pyramidal pnictogen(III) compound, the HOMO corresponds to the lone pair at the pnictogen centre, while the LUMO corresponds to two degenerate antibonding orbitals.[151] Upon deformation towards a C_s geometry the HOMO is mostly unaffected while the LUMO loses degeneracy resulting in one orbital higher in energy and one lower in energy. This causes a decrease in the HOMO-LUMO gap of the corresponding deformed pnictogen complex, potentially unlocking new reactivity. This is furthered in the deformation to C_{2v} geometry where the orbital previously corresponding to the LUMO is lowered in energy sufficiently to become the new HOMO.[151] As such, the bonding orbital in the previous geometries is now non-bonding, corresponding to a p-type vacant orbital at the pnictogen center which unlocks increased Lewis acidity. With the LUMO now going from an antibonding orbital to a non-bonding orbital there is

a significant decrease in the HOMO-LUMO gap with the ability to unlock new and potentially valuable reactivity. As in the case of group 14 compounds, perturbation away from the pyramidal geometry lowers the LUMO energy and lowers the HOMO-LUMO gap.

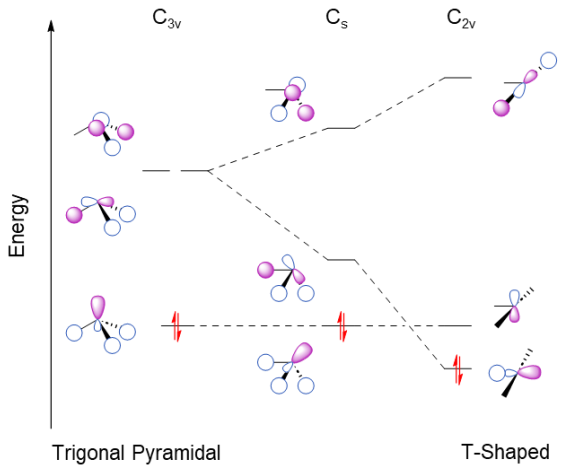

Figure 17. Qualitative Walsh diagram showing the distortion of a trigonal pyramidal pnictogen centre towards a planar T-shaped geometry.

Phosphorus

The synthesis and reactivity of non-VSEPR phosphorus compounds has seen considerable interest in recent years. An emerging constrained phosphorus platform used for catalysis is the phosphetane,[140, 151, 160] which features a phosphorus centre in a constrained ring. As this structure does not deviate significantly from the VSEPR predicted geometry at phosphorus, it is not covered here and instead the reader is referred to a recent review for more information.[28]

A key aspect of unlocking useful bond forming reactions in main group compounds is the ability to undergo oxidative addition reactions.[161] Early investigations into the reactivity of planar phosphorus compound **42** showed the ability to participate in a number of oxidative addition and other reactions.[142, 162] Some selected reactivity of this compound is shown in Figure 18, highlighting oxidative addition transformations. Compound **42** reacts with SO_2Cl_2 (or X_2 and PX_5 for the other halogens) to give the 10-P-5 species **44** with two halogen substituents at phosphorus.[142] The dichloride **44** can then be alkylated using methyl lithium to give the mono or dialkylated phosphorus compound, **45**. The dichloride can also be converted to the dihydride **48**

by reaction with $LiAlH_4$, however this species was found to be unstable and decompose via reductive elimination.[142] Another oxidative addition reaction occurs when **42** is reacted with hexafluoropropylene oxide that involves the ring opening of this epoxide to give **46**.[142] Upon heating this is converted into a species with two P-F bonds, **47**, and the loss of an unidentified fluorocarbon byproduct. The resulting species shows a slightly different geometry than that of the other halogens or alkyls with a square pyramidal type geometry rather than the trigonal bipyramidal observed for the other halogens.[142]

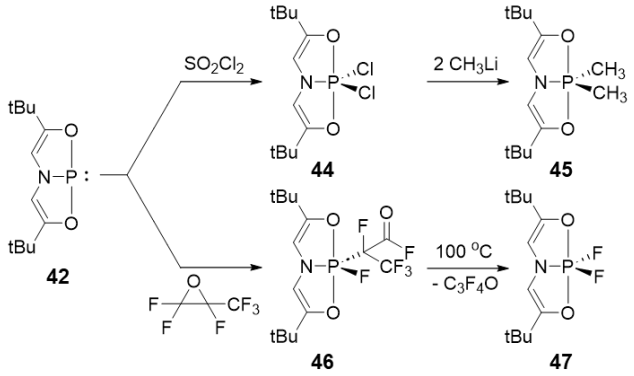

Figure 18. Selected oxidative addition type reactivity of T-shaped phosphorus compound **42**.

Research into geometrically constrained phosphorus compounds was reinvigorated in 2012 with Radosevich's report of the use of compound **42** in catalytic hydrogenation.[163] The planar phosphorus compound was able to catalyze the transfer hydrogenation of azobenzene using ammonia-borane as a source of hydrogen. The same process did not occur in the presence of traditional trigonal phosphines or phosphites and with only minor conversion in the presence of $P(NMe_2)_3$, thus suggesting the planar structure of **42** is essential to this catalytic process.[163] This reaction was proposed to proceed through a P(III)/P(V) redox couple, a catalytic redox process which is rare for main group systems (Figure 19a). In this mechanism it is proposed that the hydrogenation occurs via the dihydride intermediate **48** which transfers hydrogen to azobenzene. This mechanism is supported by NMR evidence showing **48** as the only phosphorus containing species present during the reaction, and the isolation of **48**. An alternative mechanism was later proposed based on DFT calculations whereby rather than a redox process the hydrogen is a ligand-cooperative process where the oxidation state of the phosphorus centre remains

unchanged (Figure 19b).[164, 165] In this mechanism the hydrogen is added across one of the P-O bonds of the ligand resulting in a phosphorus hydride and a proton on the oxygen which can then be transferred to azobenzene in a concerted process.[165]

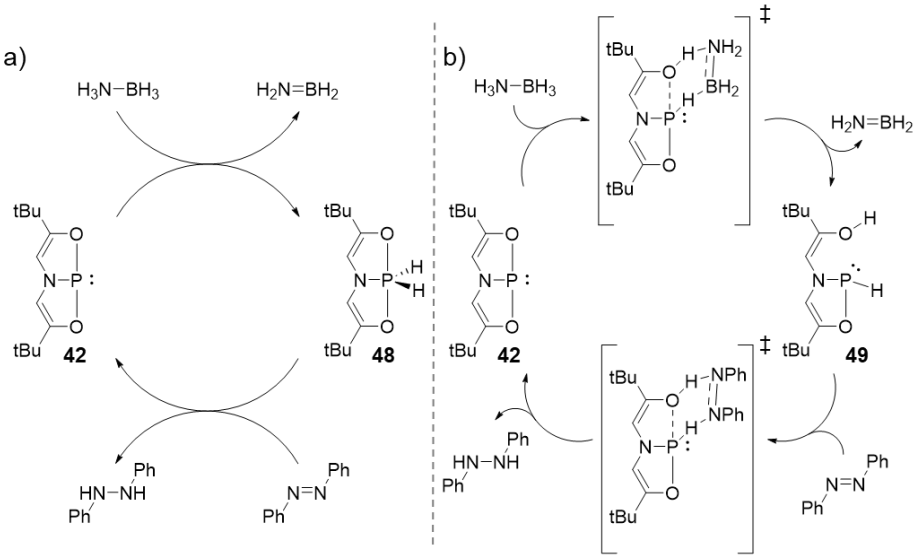

Figure 19. Catalytic transfer hydrogenation of azobenzene by T-shaped phosphorus compound **42**. a) Mechanism based on P(III)/P(V) redox couple. b) Mechanism based on ligand cooperative reactivity.

Another important chemical transformation that **42** was found to be capable of participating in is the activation of N-H bonds.[166] Under mild conditions **42** is able to add ammonia, and alkyl or aryl amines resulting in the five-coordinate phosphorus species **50**. Although attempts to reductively eliminate the N-H bond from **50** were unsuccessful even with heating and reduced pressure, the addition of an excess different amine was able to result in exchange to give a new phosphorus compound **51**.[166] The original report of this oxidative addition process suggested that this reactivity was localized on the phosphorus centre based on a combination of deuterium labelling studies and computational evidence.[166] It was suggested that due to the T-shaped nature of **42** the activation of amines can occur via an electrophilic process as the T-shaped structure engenders the phosphorus center with Lewis acidity not common to trigonal phosphines. A computational investigation has suggested this process occurs instead via a ligand cooperative pathway.[167] Regardless of the activation mechanism involved, it is clear that

the geometry constraining ligand supporting **42** is critical to unlock unique reactivity not possible for pyramidal phosphines.

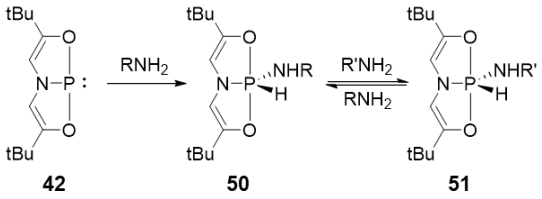

Figure 20. Activation of N-H bonds in amines by distorted phosphorus compound **42** and exchange with other amines.

A more recent distorted phosphorus platform **52** features an NNN pincer ligand which distorts the phosphorus centre into a C_s geometry rather than the planar structure exhibited by **42**.[168] This phosphorus platform was able to oxidatively add a variety of O-H and N-H bonds to give the five-coordinate phosphorus compound **53** with a distorted geometry between trigonal bipyramidal and square pyramidal. While the solid-state structures of these oxidative addition products showed a five-coordinate phosphorus centre, solution NMR studies pointed to an equilibrium between P(III) and P(V) species **53** and **54**.[168] Compound **54** can form two isomers, either *anti* or *syn*, and the ratio between all three of these is dependent on temperature.[168] As in the case of oxidative additions to **42**, these are also able to undergo exchange in the presence of an excess of a different alcohol or amine. In contrast to **42**, the oxidative addition to distorted phosphorus platform **52** is able proceed reversibly under certain conditions. In cases where R = tBu and under heating with dynamic nitrogen flow, reductive elimination occurs, an important step towards enabling a catalytic transformation.[168] Additionally, compound **52** was also shown to undergo a stoichiometric hydrodefluorination process of aryl C-F bonds via a P(V) intermediate.[169] In order to comprehensively understand the changes which occur to the frontier molecular orbitals upon deformation and explain the observed reactivity, detailed XANES and TD-DFT analysis was undertaken.[170] These support the view that decreased frontier orbital energy differences (foreshadowed in Figure 17) were crucial to the ability for phosphorus to act as both an electron-acceptor and donor.[170] Furthermore, a modification to the ligand framework of **52** to

add pyridine donors enables the distorted phosphorus centre to coordinate to a ruthenium complex or insert into a Ru-H bond.[171]

In addition to the protic O-H and N-H bonds, compound **52** was also found to be capable of activating the hydridic B-H bond in pinacolborane via a ligand cooperative pathway.[172] This B-H activation was then able to be utilized for the catalytic hydroboration of imines (Figure 21). The mechanism of this reaction was elucidated based on validated stoichiometric steps to understand how this catalytic process occurs. After the initial ligand cooperative activation of pinacolborane to give **55**, the formal insertion of an imine into the P-H bond occurs resulting in **56**.[172] The final step of this process is the intramolecular boryl transfer to eliminate the borylamine and regenerate **52**, closing the catalytic cycle.[172]

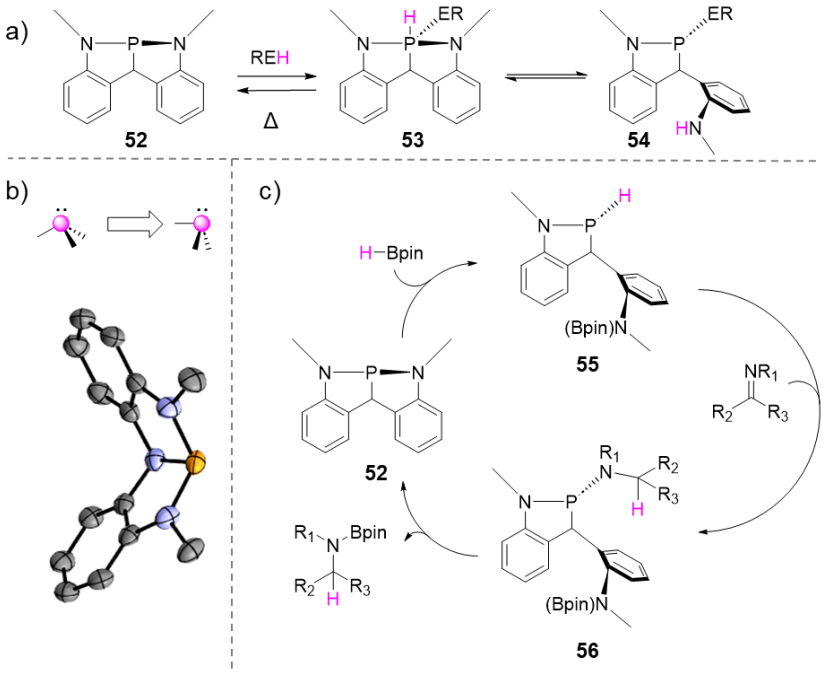

Figure 21. a) Activation of E-H bonds by geometrically constrained phosphine **52**. b) Diagram showing distortion of phosphorus centre to C_s geometry and molecular structure of **52**: CCDC #1407383. Hydrogen atoms omitted and ellipsoids set at the 50% probability level. c) Catalytic hydroboration of imines by **52**.

Several other non-VSEPR phosphorus compounds have been investigated in the last several years, with most of these featuring C_s geometries like that of **52**, rather than the fully

planar structure of **42**. One example is Kinjo's report of diazadiphosphapentalene **57**, which features two phosphorus centres in a bent bicyclic structure.[173] This compound was able to activate the N-H bond in ammonia through a σ-bond metathesis pathway to give **58** (Figure 22). This N-H activation is not reversible due to further isomerization of the N-H activation product **58**. Follow-up reactivity studies showed this compound was able to add an equivalent of H_2 from ammonia-borane and react with electrophiles.[174] Additionally, the coordination chemistry of **57** with transition metals was explored.[174] Uhl reported compound **59**, which is highly unusual for being bound to an all-carbon pincer framework arising from three sp^2 hybridized carbon atoms in a bicyclic structure.[175] This phosphorus centre is slightly bent thus forming a C_s geometry, although it is close to a planar structure with only a slight out of plane bending. Reactions of **59** with halogens resulted in the oxidative addition products such as **60** with a P(V) centre which feature a trigonal bipyramidal geometry.[175] The reactivity of **59** was further explored through reactions with chalcogens, coordination chemistry with transition metals, and notably this compound was able to insert carbon monoxide into one of the P-C bonds when reacted with a metal carbonyl.[175, 176]

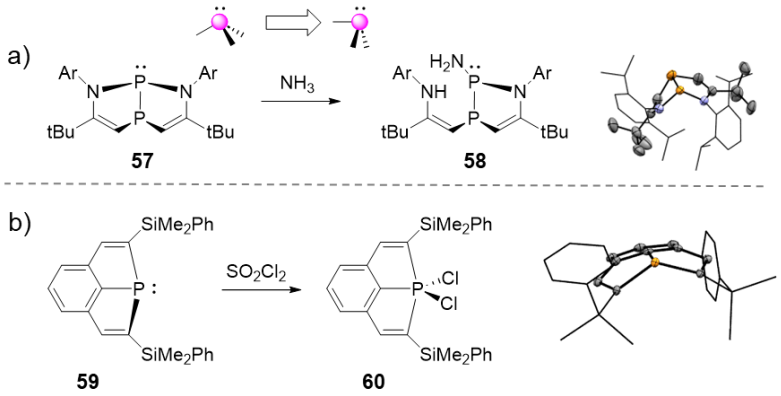

Figure 22. a) Activation of ammonia by distorted phosphorus compound **57** and molecular structure of **57**: CCDC # 1021267. b) Oxidative addition of Cl_2 to distorted phosphorus compound **59** and molecular structure of **59**: CCDC # 1582335. Hydrogen atoms omitted and ellipsoids set at the 50% probability level.

The groups of Aldridge and Goicoechea reported the compound **61**, the C_s symmetry of which is supported by an ONO ligand with phenyl rings in the backbone.[177] The reactivity of this

compound was comprehensively investigated, showing some similarities to the previously discussed compounds as well as some unique reactivity.[177-179] Compound **61** was able to activate the E-H bonds in both ammonia and water at the phosphorus centre, resulting in five-coordinate phosphorus species similar to the activation of amines by **42**.[177] Interestingly, adding an additional equivalent of **61** to the water activated product is able to activate the second O-H bond to give an oxo-bridged species.[177] The reactivity of **61** was also probed towards electrophiles and nucleophiles, finding that nucleophiles attack at the phosphorus centre (Figure 23a), while electrophiles add to the nitrogen on the ligand.[179] Sequential reaction of a nucleophile followed by an electrophile instead led to five-coordinate phosphorus species with both nucleophile and electrophile on phosphorus. The arsenic analogue of **61** was also accessed and found to behave similarly towards electrophiles and nucleophiles, aside from the inability to form five-coordinate pnictogen species.[179] The redox reactivity of **61** was also explored further, finding that the halogens could be oxidatively added to give P(V) species.[178] Additionally, **61** could be reduced by one electron resulting in a dimeric species bridged by a P-P bond.[178]

Goicoechea and co-workers later developed an asymmetric NNS ligand to access distorted phosphorus compound **63**.[180] The geometry about this phosphorus centre is similar to that of the NNN ligated **52** previously discussed as expected based on the similarities in the ligand framework. The replacement of a nitrogen donor with a sulfur was investigated as it was expected that this change should disfavour the formation of a P(V) species and instead unlock ligand-cooperative reactivity.[180] This was realized in the reactivity with amines, proceeding to give the P(III) N-H activation product **64** (and the other isomer due to hindered N-C bond rotation, Figure 23b). In contrast to **52** this does not form the P(V) species, and unlike **57** this activation is reversible, thus representing a unique ammonia activation pathway and the first of its kind among the p-block elements.[180]

By using a more rigid NNN pincer ligand a fully planar T-shaped phosphorus compound **65** was able to be accessed.[181] Due to the rigidity imparted by tethering the backbone of the ligand this compound is forced into a fully planar geometry while most similar compounds feature a C_s type geometry. The reactivity of **65** was found to be mostly similar to that of **61**, displaying ambiphilic reactivity. However in the case of **65** both nucleophiles and electrophiles add directly

to the phosphorus centre.[181] Compound **65** is able to be oxidized by oxygen, sulfur, selenium or azides to give the corresponding P(V) species featuring a double bond to the chalcogen or nitrogen atom.[181] Reactions of **65** with a variety of protic and hydridic E-H bonds also occur in a ligand cooperative manner where the phosphorus centre remains P(III), reminiscent of those with **52**. In all cases the electropositive atom adds to the ligand nitrogen while the electronegative atom adds to the phosphorus centre, as demonstrated for the reaction with HCl yielding compound **66** (Figure 23c).[181]

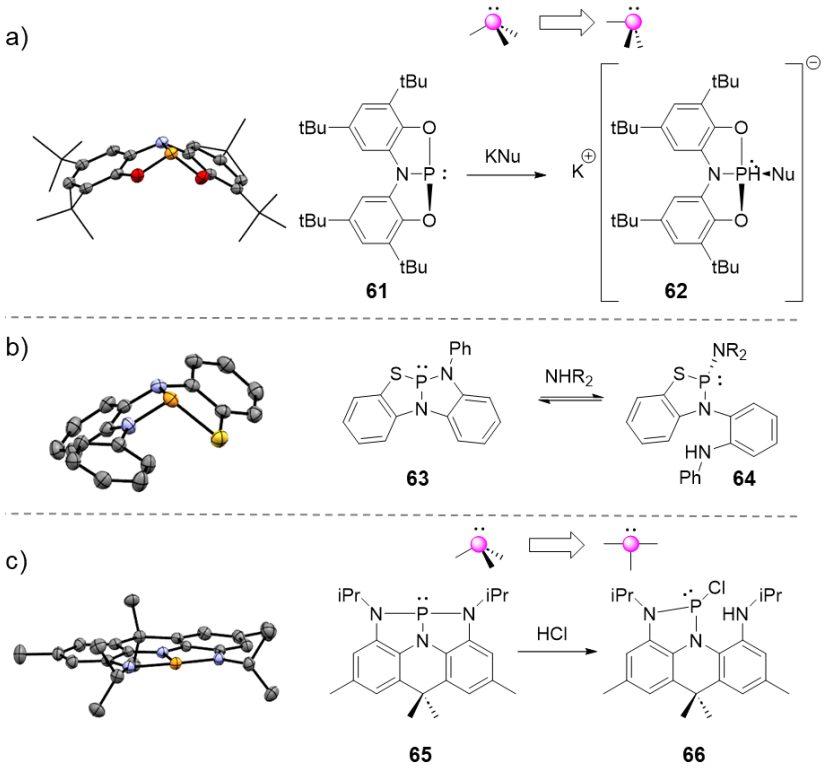

Figure 23. a) Reactivity of **61** towards nucleophiles (Nu = OtBu or NPh_2) and molecular structure of **61**: CCDC # 1415185 b) Reversible activation of the N-H bond of amines by **63** and molecular structure of **63**: CCDC # 2097495 c) Ligand-cooperative reaction of **65** with HCl and molecular structure of **65**: # 2245885. Hydrogen atoms omitted and ellipsoids set at the 50% probability level.

While most of the distorted phosphorus compounds discussed thus far have focused on neutral, tricoordinate species there is emerging interest in geometrically constrained phosphorus centres which bear charge. One example is the ONO coordinated phosphenium cation **67**

reported by Dobrovetsky which displays ambiphilic reactivity.[182] This phosphorus centre bears a C_s geometry, very similar to that of the neutral **61** discussed above. In contrast to non-constrained phosphenium cations, **67** oxidatively adds water or alcohols to give the phosphonium cation **68** featuring a five-coordinate phosphorus centre (Figure 24).[182] Compound **67** is also able to activate the N-H bond of ammonia to give the oxidative addition product **69**. Remarkably, this oxidative addition is reversible, and upon heating the phosphenium cation **67** is regenerated with the loss of ammonia.[182]

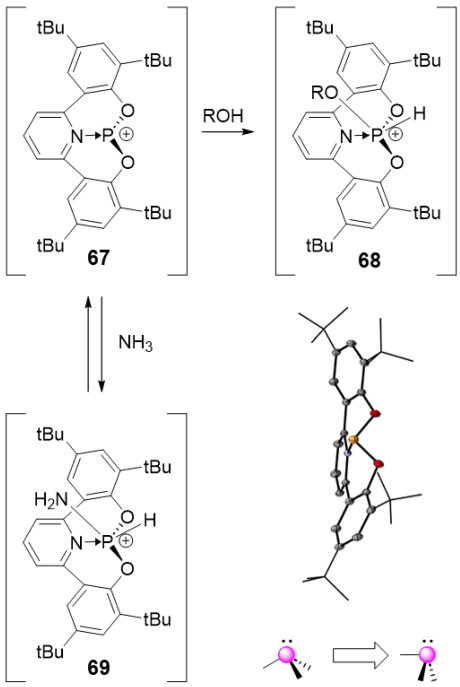

Figure 24. Reactivity of distorted phosphenium cation **67** towards alcohols and ammonia (R = H, Me, iPr, tBu), with molecular structure of **67**: CCDC # 1831470. Hydrogen atoms omitted and ellipsoids set at the 50% probability level.

A similar geometrically constrained phosphenium cation **70** supported by an NNN ligand framework was also recently reported by Dobrovetsky and co-workers.[183] Similar to **67**, this compound was also capable of activating E-H bonds, but instead this proceeded via a ligand assisted pathway with the phosphorus centre remaining P(III) as shown for the addition of methanol to give **71** (Figure 25).[183] Phosphenium cation **70** was also able to add an equivalent of H_2 from ammonia-borane in a ligand cooperative fashion forming a similar P(III) compound.

Reaction of **70** with triethylsilane proceeded with the elimination of Et_3SiOTf, indicating that the anion interferes with the reactivity. Exchanging the triflate anion for $B(C_6F_5)_4^-$ enabled the oxidative addition of triethylsilane to give **72**, which rapidly decomposed.[183] In contrast to the other oxidative addition products, NMR data suggested **72** is a P(V) species where both the hydride and silicon are bound directly to the phosphorus centre. Although **72** was short-lived, this oxidative addition was able to be utilized in the catalytic hydrosilylation of benzaldehyde.[183] It was proposed based on NMR evidence that this catalytic cycle goes first via oxidative addition to give **72**, followed by phosphasilylation to **73**, and finally reductive elimination to form the silyl ether and regenerate **70**.[183] The constrained geometry of **70** is essential to unlocking this unique and valuable transformation as phosphenium cations are generally not able to react in this ambiphilic manner.

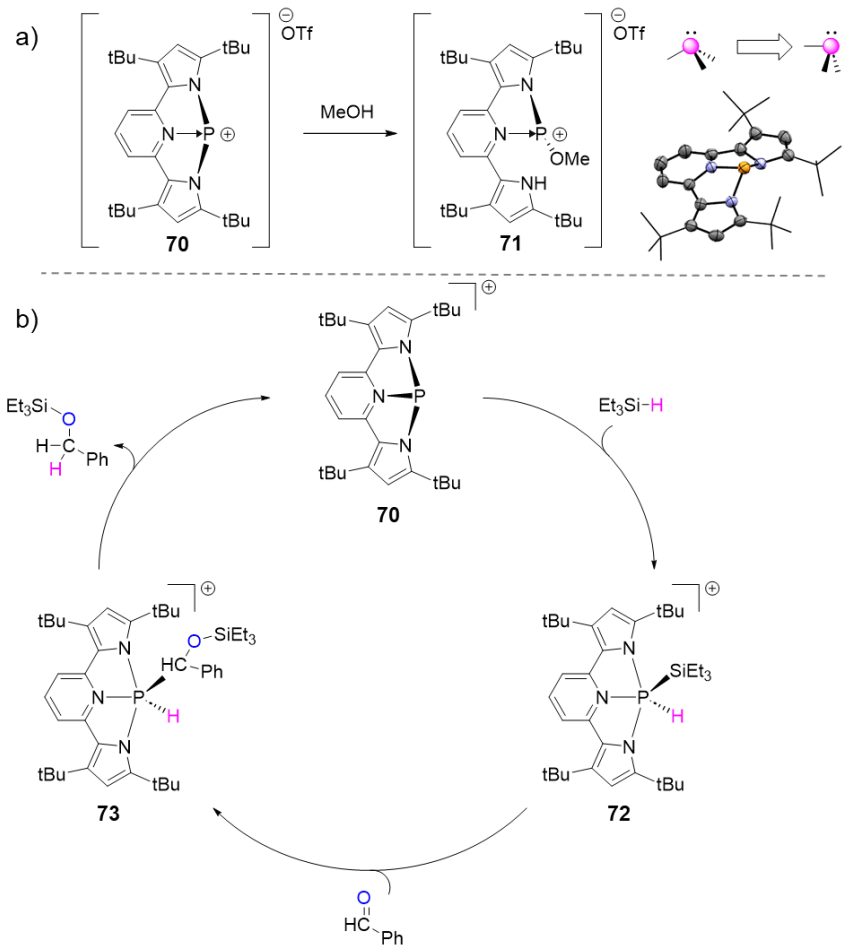

Figure 25. a) Ligand cooperative activation of methanol by constrained phosphenium cation **70** and molecular structure **70**: CCDC # 2159232. Hydrogen atoms omitted and ellipsoids set at the 50% probability level. b) Catalytic hydrosilylation of benzaldehyde by constrained phosphenium cation **70**.

Another unique constrained phosphorus compound is the four-coordinate anionic phosphoranide **74**.[184-186] Typical phosphoranide species are 'see-saw' shaped or trigonal bipyramidal if considering the lone pair as a substituent, while the constrained ligand in **74** forces this molecule into a square pyramidal geometry.[185] Unsurprisingly, reaction with electrophilic methyl iodide gave the five-coordinate phosphorus species **75**. More interestingly, reaction of **74** with benzophenone resulted in tetraphenyl epoxide and the phosphorane hydroxide **76**.[185] This type of reactivity is unprecedented for phosphoranides which usually undergo nucleophilic addition to carbonyls. Additionally, when **74** is reacted with I_2 a dimeric species featuring a P-P bond is formed in contrast to typical phosphoranides which generally form halophosphoranes.[185] These two reactions suggest that **74** is capable of undergoing redox chemistry and are specifically indicative of single electron transfer processes. In order to confirm this process a radical of **74** was able to be trapped by benzophenone and studied using EPR spectroscopy to confirm this as a possible pathway.

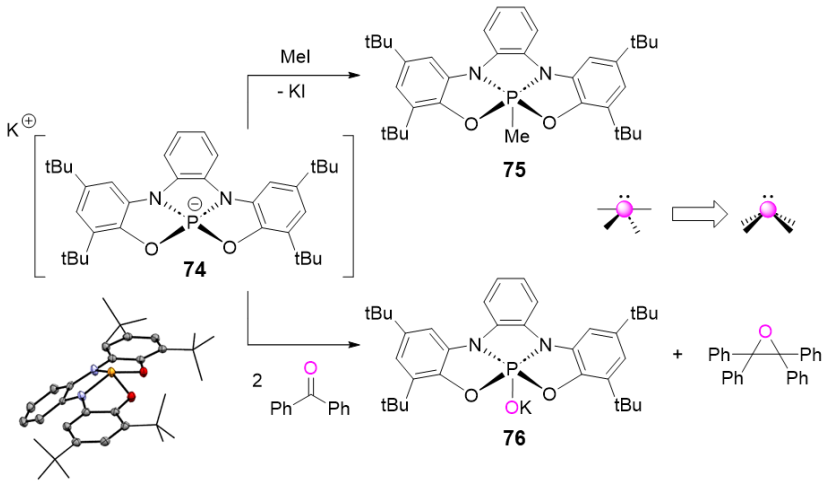

Figure 26. Reactivity of **74** with MeI and benzophenone, and molecular structure of **74**: CCDC # 2122222. Hydrogen atoms omitted and ellipsoids set at the 50% probability level.

Another cationic geometrically distorted phosphorus system **77** has been reported for the catalytic hydrodefluorination and amination of aryl-F bonds (Figure 27).[187] The bismuth analogue of this compound was previously reported, also featuring distorted bond angles, however less pronounced due to the larger size of the bismuth atom allowing for more flexibility.[188] While **77** did not react with amines, alcohols, or silanes unlike many of the previously discussed distorted phosphorus compounds, it was found to react with electron-poor aryl fluorides. This reactivity was exploited for the catalytic hydrodefluorination and C-N cross-coupling on electron deficient fluoroarenes.[187] As highlighted in Figure 27, these catalytic reactions proceeded stepwise via a process common to transition metals, but rarely observed for main group element centres. The first step is oxidative addition at the phosphorus centre to form the P(V) **78**, followed by a ligand metathesis reaction where the fluoride is exchanged with a silyl hydride or silylamine to give **79**. Finally a reductive elimination occurs to yield the desired product and regenerate the catalytic species **77**.[187]

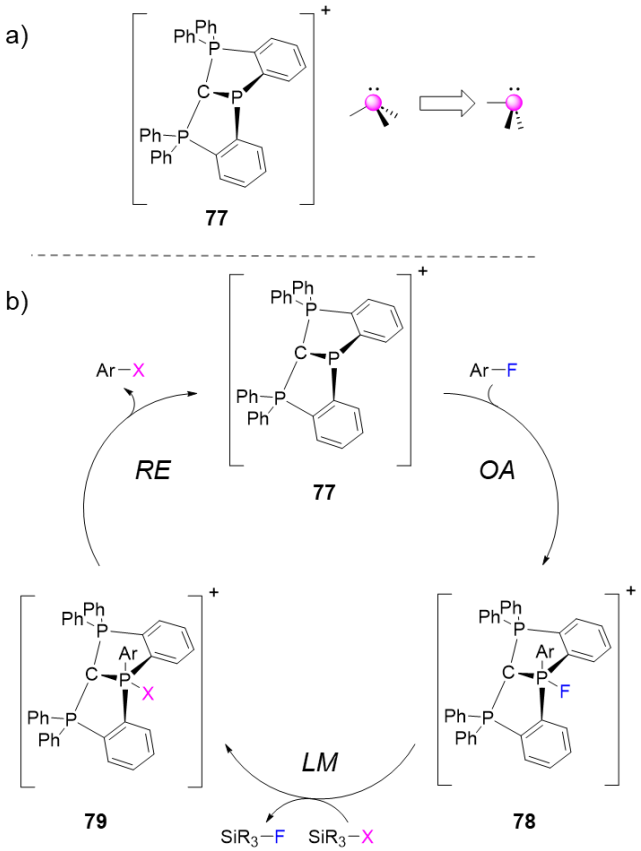

Figure 27. a) Geometrically distorted phosphorus cation **77** b) Catalytic cycle showing hydrodefluorination and C-N cross-coupling reactivity of **77**.

Arsenic, Antimony, and Bismuth

The chemistry of the heavier pnictogens in non-VSEPR conformations has been much less explored than that of phosphorus, however there are still some notable examples. Bismuth (I) compounds have gained considerable attention recently for their emerging catalytic properties.[156, 157, 189-196] However, due to the low-valent nature of these compounds their planar geometry is VSEPR consistent and thus falls outside the scope of this review.

Arduengo and co-workers reported the first planar T-shaped arsenic and antimony compounds **80** and **81** shortly after the report of the first planar phosphorus compound **42**.[197-199] The reactivity of these heavier systems was like that of phosphorus but with some key structural differences that provide some insight into their differing electronic structures. Oxidation of the antimony complex **81** by chlorine yields a square based pyramidal compound **81Cl$_2$** (Figure 28), which is interpreted as retaining a lone pair and therefore a +3 oxidation state.[197] In contrast, the chlorinated phosphorus compound **44** (accessible by chlorination of **42**) shows a trigonal bipyramidal geometry interpreted as having no lone pairs and therefore a +5 oxidation state. (Figure 28).[197] Based on these structural differences, **81** may be interpreted as featuring an antimony centre in the +1 oxidation state (2 lone pairs), and **42** as featuring a phosphorus centre in its +3 oxidation state (1 lone pair). Similarly, when coordinating to transition metals the phosphorus analogue is able to adopt a bent geometry, while **81** remains planar due to coordination via one of its two lone pairs, thus giving different geometries in the transition metal complexes.[197, 200] This apparently enhanced stability of the lower oxidation states for heavier elements reflects expected periodic trends.

Another set of T-shaped pnictogen complexes are the radical anions of phosphorus, arsenic, and antimony **82-84** reported by Wang and co-workers.[201] For all three of these complexes both the neutral analogues and radical anions were able to be accessed, however the bismuth derivatives were not reported. These compounds adopt a purely planar geometry around the pnictogen centre due to the highly rigid nature of the NNN pincer ligand used. The

electronic structure of these compounds were comprehensively probed, determining the unpaired electron is largely localized at the pnictogen centre.[201] Furthermore, the arsenic and antimony derivatives **83** and **84** reacted with sulfur to produce the S_{10}^{2-} dianion and the neutral pnictogen complex.[201]

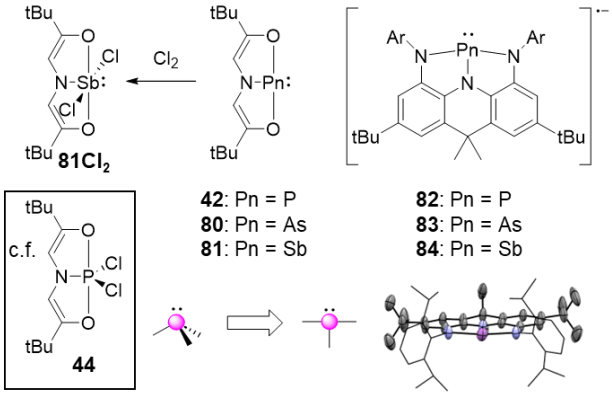

Figure 28. Planar T-shaped pnictogen complexes supported by tridentate pincer ligands and molecular structure of **84**: CCDC # 1936157. Hydrogen atoms omitted and ellipsoids set at the 50% probability level. Reaction of **81** with Cl_2 also shown and comparison with the phosphorus analogue.

A recent study by Chitnis and co-workers focusing on a series of pnictogen triamides provides insight into the differences descending the group.[202] It was found that for the lighter phosphorus and arsenic derivatives, **85P** and **85As**, the flexibility of this ligand framework allowed for a bent structure to be adopted (<N-P-N-N = 110.6 ° and <N-As-N-N = 110.2 °). [202] In contrast, the heavier antimony and bismuth derivatives, **85Sb** and **85Bi** were planar in solution (<N-Sb-N-N = 179.9 ° and N-Bi-N-N = 180.0 °), while the antimony derivative **85Sb** adopted a dimeric structure in the solid state.[202] This difference in geometry was realized in the intrinsic properties of these compounds as bent **85P** and **85As** are colourless while the planar **85Sb** and **85Bi** are intensely coloured (Figure 29b). In order to explain the trend of this structural preference for planarization in the heavier analogues but not the lighter analogues, extensive DFT calculations were undertaken. It was determined that for **85Sb** and **85Bi** the planar geometry is stabilized by increased orbital stabilization of the 3-center-4-electron bond due to the increased electronegativity differences between nitrogen and the antimony or bismuth centre.

Destabilization of the planar geometry for **85P** and **85As** is provided by an increased penalty from electrostatic interactions when compared to **85Sb** or **85Bi**.[202] This change in geometry is found to be important when considering the reactivity of the resulting compounds. The bent phosphorus and arsenic compounds show no reaction with Lewis bases while the planar bismuth and antimony compounds are Lewis acids able to coordinate two equivalents of pyridine n-oxide. This can be explained by the planarization revealing a vacant low-lying orbital at the pnictogen center, thus enabling unique reactivity.

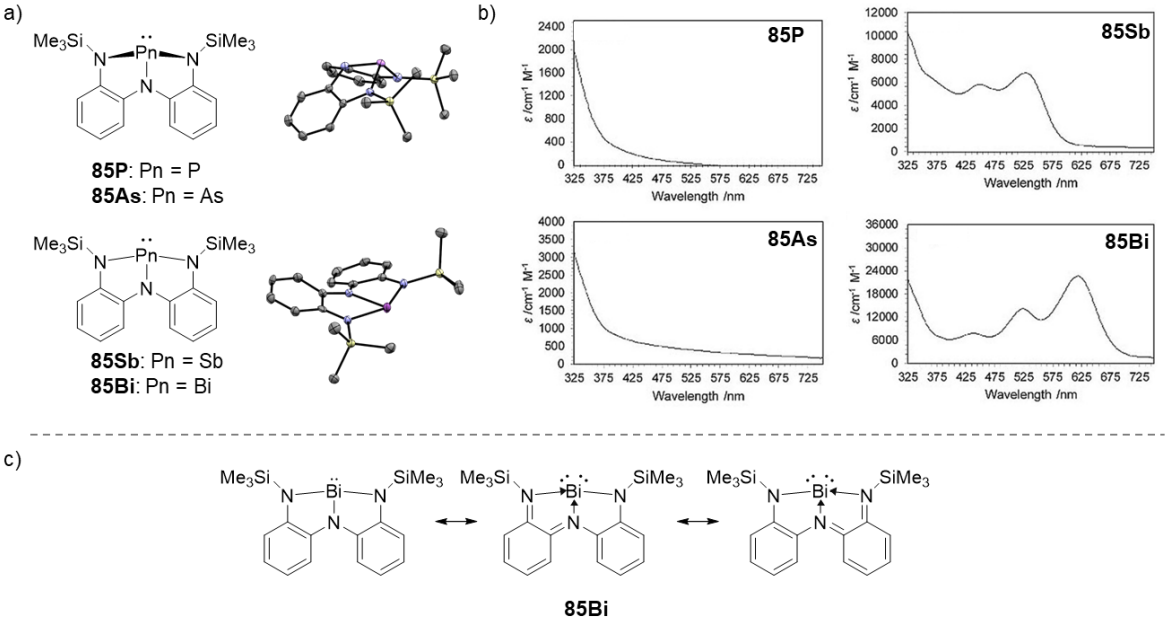

Figure 29. a) Bent phosphorus and arsenic triamides and planar antimony and bismuth triamides **85Pn** (Pn = P, As, Sb, and Bi) and representative molecular structures of **85As**: CCDC # 1949723; and **85Bi**: CCDC # 1893377. Hydrogen atoms omitted and ellipsoids set at the 50% probability level. b) UV-Vis spectra of compounds **85P-85Bi**. c) Resonance structures of planar bismuth triamide **85Bi**.

The planar bismuth compound **85Bi** was the first report of a planar, neutral, trivalent bismuth centre.[203] Note that Arduengo's earlier attempts to extend ONO-pincer chemistry to bismuth were unsuccessful, instead leading to a 20-Bi-9 system where three equivalents of the ligand are coordinated to bismuth, likely due to the large size of bismuth and the poor steric protection afforded by this ligand.[204] The sterically better shielded **85Bi** is T-shaped, with the

constrained geometry supported by a redox-active NNN pincer ligand framework. Much like in the previously discussed T-shaped phosphorus compound **42**, the geometry of **85Bi** can be explained by considering resonance structures (Figure 29c). Due to the redox-active nature of the ligand this compound can be considered to be in either the Bi(III) or Bi(I)[152] oxidation state. The bismuth (I) resonance structure has two lone pairs of electrons at the bismuth centre and thus should favor the formation of the observed T-shaped geometry (Figure 29c). Participation of both resonance structures in the observed properties of this molecule led to its description as 'redox-confused' where the electronic structure and bonding is reminiscent of a Bi(I) species, but its reactivity is similar to that expected of B(III) compounds.[203] Andrada and Salvador have offered an alternative understanding of the electronic structure of such compounds based on electron richness/poorness rather than formal oxidation states.[205] Follow-up studies on this system investigated the introduction of electron withdrawing substituents on the ligand framework in order to increase the Lewis acidity at bismuth. Initial computational studies predicted an increase in Lewis acidity[205, 206] which was later realized experimentally in a number of complexes bearing electron withdrawing groups such as bromines and sulfonamides (compounds **86**-**88**, Figure 30).[207] Depending on the substituents these complexes display tuneable Lewis acidity, with the strongest bearing Lewis acidity comparable to that of fluorinated triarylboranes. Additionally, these planar bismuth complexes were capable of initiating the polymerization of lactones to produce polymers with high molecular weights and excellent dispersity.[207]

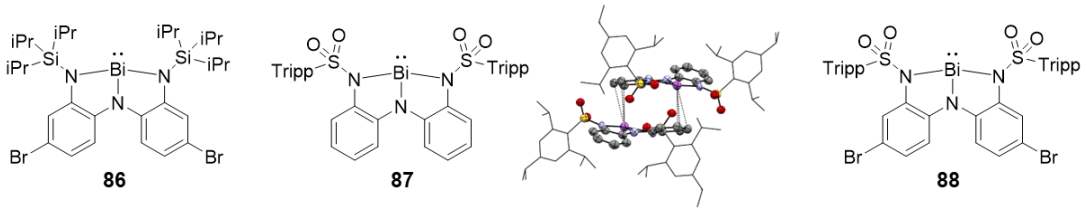

Figure 30. Electronic and structural variations for planar bismuth compounds and dimeric structure of **87** CCDC # 2217453.

Additional related studies investigated the effect of mesomeric tuning on these bismuth complexes by exchanging one of the nitrogen donors in the tridentate ligand for a carbon.[208] It was predicted that a reduction in π-donation to bismuth from the carbon atom in the ligand would lower the LUMO energy of these complexes and thus result in stronger electrophilic

character at the metal centre. Attempts to isolate these NCN bismuth (III) complexes **89R** in monomeric form were unsuccessful. In cases where the ligand substituents were bulky (R = 2,6-diisopropylphenyl) a reduction process was observed with the loss of H_2 to give bismuth (I) compound **90**. When less sterically demanding substituents (R = $SiMe_3$) were used a dimerization process was instead observed where a nitrogen atom bridged two bismuth centres to give **91**. These results indicate that the desired product **89R** is clearly more electrophilic than **88** as it cannot be isolated without having this electrophilicity quenched via either reduction or dimerization. Interestingly, it was possible to detect monomeric derivatives of **89R** as the dominant species in the gas phase by mass spectrometry, indicating they can be formed transiently or under ultra-low concentrations.

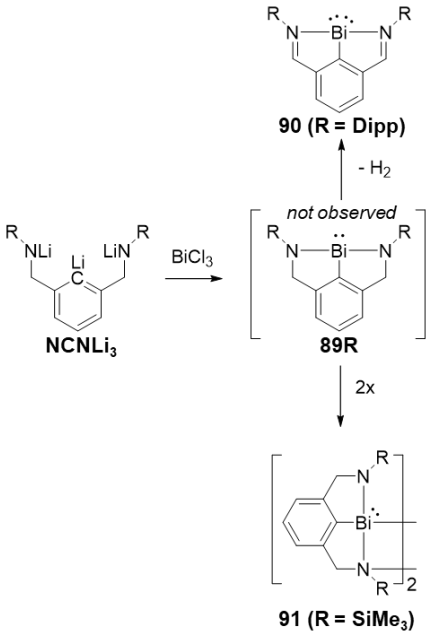

Figure 31. Attempted isolation of distorted NCN bismuth (III) complex **89R** and either reduction to Bi(I) **90** or dimerization to **91**.

A unique geometrically constrained antimony compound **92** was able to be accessed using the geometrically constraining calix[4]pyrrole ligand.[209] This complex features a four-coordinate anionic antimony centre in a square pyramidal geometry. The reactivity of this compound was not investigated comprehensively, however its oxidation to a cationic antimony complex was explored and it was found that this cationic antimony complex was a Lewis superacid.[209] A related

antimony complex supported by a corrole ligand was reported previously, showing a similar distortion to square pyramidal.[210] Compound **93** was able to be oxidized to the Sb(V) derivative by using halides, and it was shown these halogens could be photoeliminated, returning to the Sb(III) compound, representing a rare example of photo-triggered redox reversibility.

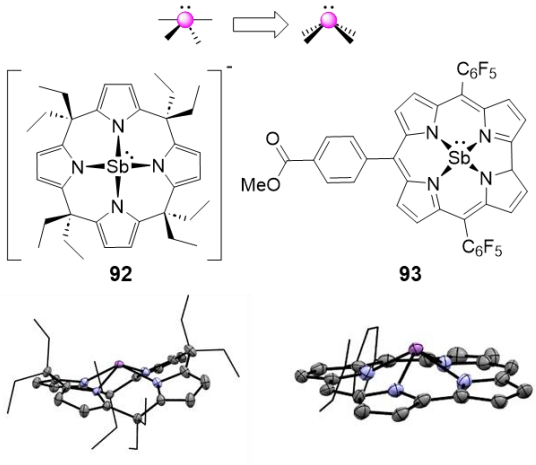

Figure 32. Geometrically constrained antimony complexes **92** and **93** and their molecular structures **92**: CCDC # 2108301, **93**: CCDC # 1049494. Hydrogen atoms omitted and ellipsoids set at the 50% probability level, C_6F_5 groups omitted from **93** for clarity.

Compounds with a Group 16 Central Element

While less common than group 13, 14, or 15, a handful of geometrically distorted group 16 compounds have also been reported and will be briefly outlined here. One interesting example of main group compounds which feature geometric deformation supported by a pincer ligand are the 10-Ch-3 dioxachalcapentalenes (where Ch = chalcogen) **94-96**.[211-214] These compounds are isostructural to the previously discussed 10-Pn-3 compound of Arduengo, with a T-shaped main group centre supported by a tridentate ligand. While the pnictogen complexes of Arduengo can undergo 'electromorphism' between the T-shaped 10-Pn-3 structures and bent 8-Pn-3 structures, this is not possible for the chalcogens which prefer the 10-Ch-3 bonding configuration (Figure 33).[197] This is clear from the resonance structures shown as the 8-Ch-3 configuration features an unfavourable charge separation with a positive charge at the chalcogen centre and an unstablized carbanion.[197] As chalcogen species **94-96** are in the + 4 oxidation state and feature a lone pair, these can be considered to be non-VSEPR structures much like the analogous 10-Pn-3

compounds. In contrast, other pincer supported chalcogen compounds **97-99** are in the + 2 oxidation state and are largely VSEPR consistent due to the two lone pairs present.[215-217]

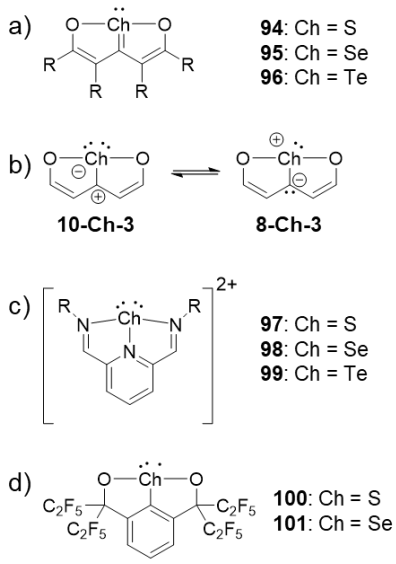

Figure 33. a) Geometry distorted chalcogen compounds **94-96**. b) Difference between favorable 10-Ch-3 and unfavorable 8-Ch-3 structures. c) Related pincer chalcogen compounds which are similar to VSEPR predicted geometry. d) Geometrically constrained sulfuranyl radicals.

Other geometrically distorted group 16 species include T-shaped radicals **100** and **101** which are supported by pincer ligands. The chemistry of sulfur-centered radicals has been extensively studied, including those of the sulfuranyl radicals (sulfur centered radicals containing nine formal electrons and a coordination number of three).[218, 219] The bonding character of these radicals can exist in multiple forms including a pyramidal case featuring a 2-centre-3-electron bond, or T-shaped cases with either a 3-centre-3-electron bond (σ-type) or 3-centre-4-electron bond (π-type).[220] Sulfuranyl radicals featuring this T-shaped geometry can be considered to be non-VSEPR species, however due to their low stability these are most often considered as intermediates. A T-shaped sulfuranyl radical was reported in 1986 as a 9-S-3 system which was isolable and thermally stable due to the supporting pincer ligand.[221] This initial report was similar to **100** but featured CF_3 groups in place of the C_2F_5 groups. This was later expanded to the selenium derivative **101** as well, with the C_2F_5 groups added to increase the barrier to

dimerization of these species. Compound **100** was found to be able to be redox interconverted to the anion or cation, thus showing potential as an organic radical battery.[220]

Summary and Outlook

While reliable prediction of molecular geometry using first heuristic (e.g. VSEPR) and later quantitative models (e.g. QTAIM and MO theory) was a crowning of 20th century structural inorganic chemistry, it is now clear that deliberate treatment of geometry itself as a *variable* – rather than a prescribed outcome – offers a rich vein of inquiry. Alongside steric and electronic tuning, geometric tuning thus also emerges as a means of rationally controlling chemical outcomes (Figure 34). The pincer ligand approach to exert geometric control owes a great debt to the more mature field of transition metal coordination chemistry, from which the notion of multi-dentate ligands has now been fully adopted for use in the p-block. Meanwhile, the development of ever-bulkier substituents, first motivated by the desire to isolate fragile low-coordinate or low-oxidation state species, has also found usage in geometric distortion via inter-ligand repulsion. Lastly, the use of electron-donation intramolecularly via the σ or π framework, or intermolecularly via external ligands is also a viable route to accessing molecules with non-classical geometries often with short lifespans. As the example of lone-pair or π-bond free 1-boraadamantane (compound **1**) shows, it is almost impossible to escape intramolecular electron-donation into any vacant orbitals that geometric distortion generates. Indeed, in essentially all cases, more than one of the above general approaches is operative.

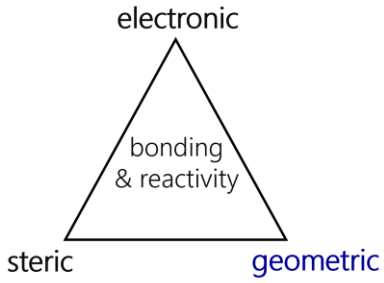

Figure 34. Avenues to controlling the bonding and reactivity of a p-block element centre.

Geometric perturbation has the ability to unlock unprecedented reactivity, as illustrated by the discovery of high Lewis acidity for square planar aluminates and silicon hydride anions,

and challenging redox processes (both stoichiometric and catalytic) at deformed group 15 centres. While numerous catalytic applications have been developed for deformed group 15 compounds, future breakthroughs are expected by parallel studies for group 13, 14 and 16 compounds. Breakthroughs in this field are also anticipated from continued evolution of new multidentate frameworks. For example, π-donating N or O containing frameworks currently dominate the mutidentate ligand space, but the incorporation of heavier elements into ligand backbones (e.g. in compounds **57** and **63**) may reveal interesting variations in electronic structure due to the differing donor abilities and bond strengths of these elements. Similarly, heteroatom-free, all-carbon, multi-dentate substituents (e.g. in compound **1** and **59**) are very rare and represent an opportunity for new discoveries if synthetic challenges in accessing such frameworks can be overcome, as illustrated recently in the context of osmium chemistry.[222, 223] In the context of growing the multidentate frameworks used, chemists may find motivation from the field of ion sensing, where cooperative binding by construction of rigid hemispheric or macrocyclic molecules is a well-established strategy for boosting ion affinities.[224, 225] Development of even bulkier ligands is also expected, but in order to enforce non-classical geometries by repulsion, strong (attractive) dispersion donors such as aryl groups must be avoided.[22, 26, 226, 227] Studies revealing the influence of geometry on stoichiometric and catalytic reactivity described in preceding sections have to-date focused exclusively on molecular systems. It is likely that unexpected new materials properties will also emerge by embedding non-VSEPR p-block element centres into macromolecular systems like polymers and networks, which remains unprecedented.

Acknowledgements

TJH acknowledges the Natural Science & Engineering Research Council of Canada (NSERC) for a graduate scholarship. SSC acknowledges NSERC, Dalhousie University, and the Alfred P. Sloan Foundation for funding in support of this work. The authors thank all researchers whose chemistry is covered here, and reviewers for their efforts to make this a more useful overview of the field.

Profiles

Tyler J. Hannah obtained a B.Sc. from the University of Calgary (2021) working under the supervision of Warren Piers and is currently an Alexander Graham Bell (NSERC CGS-D) PhD candidate at Dalhousie University in Halifax, Nova Scotia, Canada. Tyler's research interests while working under the supervision of Saurabh Chitnis focus on the stabilization of heavy p-block elements in non-VSEPR geometries.

Saurabh S. Chitnis obtained his Ph.D. with Neil Burford at the University of Victoria (2015), where his doctoral thesis was recognized with a Governor General's Gold Medal. He then performed postdoctoral research with Ian Manners at the University of Bristol as a Banting Postdoctoral Fellow (2015-2017) and later with Doug Stephan at the University of Toronto (2017-2018). He started his independent career in main group chemistry at Dalhousie University in July 2018, where in 2023 he received tenure and was promoted to Associate Professor. He has been profiled in *Chemical Communications* as an Emerging Investigators (2020) and in *Dalton Transaction* as a New Talents (2020). More recently, he received the Dalhousie University Science Killam Prize (2023), the CNC-IUPAC National Travel Award (2023), and the Alfred P. Sloan Fellowship (2023)

References

1. R. J. Gillespie, *Coord. Chem. Rev.*, 2008, **252**, 1315-1327.
2. R. J. Gillespie and R. S. Nyholm, *Quarterly Reviews, Chemical Society*, 1957, **11**, 339-380.
3. N. V. Sidgwick and H. M. Powell, *Proceedings of the Royal Society of London. Series A. Mathematical and Physical Sciences*, 1940, **176**, 153-180.
4. J. E. Lennard-Jones, *Transactions of the Faraday Society*, 1929, **25**, 668-686.
5. A. D. Walsh, *J. Chem. Soc. (Resumed)*, 1953, DOI: 10.1039/JR9530002260, 2260-2266.
6. A. D. Walsh, *Journal of the Chemical Society (Resumed)*, 1953, DOI: 10.1039/JR9530002266, 2266-2288.
7. A. D. Walsh, *Journal of the Chemical Society (Resumed)*, 1953, DOI: 10.1039/JR9530002288, 2288-2296.
8. A. D. Walsh, *J. Chem. Soc. (Resumed)*, 1953, DOI: 10.1039/JR9530002296, 2296-2301.
9. A. D. Walsh, *J. Chem. Soc. (Resumed)*, 1953, DOI: 10.1039/JR9530002301, 2301-2306.
10. A. D. Walsh, *Journal of the Chemical Society (Resumed)*, 1953, DOI: 10.1039/JR9530002306, 2306-2317.
11. B. M. Gimarc, *Acc. Chem. Res.*, 1974, **7**, 384-392.
12. L. C. Allen, *Theoretica chimica acta*, 1972, **24**, 117-131.
13. E. A. Robinson, S. A. Johnson, T.-H. Tang and R. J. Gillespie, *Inorg. Chem.*, 1997, **36**, 3022-3030.
14. L. S. Bartell, *J. Chem. Educ.*, 1968, **45**, 754.
15. R. G. Pearson, *Journal of the American Chemical Society*, 1969, **91**, 4947-4955.
16. U. Öpik and M. H. L. Pryce, *Proceedings of the Royal Society of London. Series A. Mathematical and Physical Sciences*, 1957, **238**, 425-447.
17. H. A. Jahn, E. Teller and F. G. Donnan, *Proceedings of the Royal Society of London. Series A - Mathematical and Physical Sciences*, 1937, **161**, 220-235.
18. R. F. W. Bader, R. J. Gillespie and P. J. MacDougall, *Journal of the American Chemical Society*, 1988, **110**, 7329-7336.
19. R. J. Gillespie, *J. Chem. Educ.*, 1970, **47**, 18.
20. M. E. O'Reilly and A. S. Veige, *Chem. Soc. Rev.*, 2014, **43**, 6325-6369.
21. P. P. Power, *J. Organomet. Chem.*, 2004, **689**, 3904-3919.
22. P. P. Power, *Organometallics*, 2020, **39**, 4127-4138.
23. D. L. Kays, *Chem. Soc. Rev.*, 2016, **45**, 1004-1018.
24. K. Gour, M. K. Bisai and S. S. Sen, *Eur. J. Inorg. Chem.*, 2022, **2022**, e202200071.
25. H. B. Wedler, P. Wendelboe and P. P. Power, *Organometallics*, 2018, **37**, 2929-2936.
26. D. J. Liptrot and P. P. Power, *Nature Reviews Chemistry*, 2017, **1**, 0004.
27. J. Abbenseth and J. M. Goicoechea, *Chem Sci*, 2020, **11**, 9728-9740.
28. J. M. Lipshultz, G. Li and A. T. Radosevich, *Journal of the American Chemical Society*, 2021, **143**, 1699-1721.
29. S. Kundu, *Chem. Asian J.*, 2020, **15**, 3209-3224.
30. R. Jambor and L. Dostál, *Top. Organomet. Chem.*, 2013, **40**, 175-202.
31. H. Ruppert, L. M. Sigmund and L. Greb, *Chem. Commun.*, 2021, **57**, 11751-11763.
32. G. Bouhadir and D. Bourissou, *Chem. Soc. Rev.*, 2004, **33**, 210-217.
33. A. Maiti, R. Yadav and L. Greb, in *Adv. Inorg. Chem.*, Academic Press, 2023, DOI: https://doi.org/10.1016/bs.adioch.2023.08.006.
34. B. M. Gimarc, *Journal of the American Chemical Society*, 1971, **93**, 593-599.
35. A. V. Pomogaeva and A. Y. Timoshkin, *ACS Omega*, 2022, **7**, 48493-48505.
36. M. El-Hamdi, M. Sola, J. Poater and A. Y. Timoshkin, *J. Comput. Chem.*, 2016, **37**, 1355-1362.
37. B. M. Mikhailov and V. N. Smirnov, *Izv. Akad. Nauk SSSR, Ser. Khim.*, 1973, 2165.

38. B. Mikhailov, T. Baryshnikova, V. G. Kiselev and A. Shashkov, *Izv. Akad. Nauk SSSR, Ser. Khim*, 1979, **28**, 2544-2551.
39. M. E. Gurskii, S. Y. Erdyakov, T. V. Potapova and Y. N. Bubnov, *Russ. Chem. Bull.*, 2008, **57**, 802-814.
40. B. M. Mikhailov, *Pure Appl. Chem.*, 1983, **55**, 1439-1452.
41. S. S. Bukalov, L. A. Leites, Y. N. Bubnov, M. E. Gurskii and T. V. Potapova, *Bulletin of the Academy of Sciences of the USSR, Division of chemical science*, 1989, **38**, 426-427.
42. Y. V. Vishnevskiy, M. A. Abaev, A. N. Rykov, M. E. Gurskii, P. A. Belyakov, S. Y. Erdyakov, Y. N. Bubnov and N. W. Mitzel, *Chem. Eur. J.*, 2012, **18**, 10585-10594.
43. L. S. Bartell and B. L. Carroll, *The Journal of Chemical Physics*, 2004, **42**, 3076-3078.
44. B. Wrackmeyer and O. L. Tok, *Zeitschrift für Naturforschung B*, 2005, **60**, 259-264.
45. T. Laube and E. Schaller, *Acta Crystallographica Section B*, 1995, **51**, 177-181.
46. K. T. Giju, A. K. Phukan and E. D. Jemmis, *Angew. Chem. Int. Ed.*, 2003, **42**, 539-542.
47. A. Chardon, A. Osi, D. Mahaut, T. H. Doan, N. Tumanov, J. Wouters, L. Fusaro, B. Champagne and G. Berionni, *Angew. Chem. Int. Ed. Engl.*, 2020, **59**, 12402-12406.
48. T. K. Wood, W. E. Piers, B. A. Keay and M. Parvez, *Org. Lett.*, 2006, **8**, 2875-2878.
49. A. Ben Saida, A. Chardon, A. Osi, N. Tumanov, J. Wouters, A. I. Adjieufack, B. Champagne and G. Berionni, *Angew. Chem. Int. Ed.*, 2019, **58**, 16889-16893.
50. A. Osi, D. Mahaut, N. Tumanov, L. Fusaro, J. Wouters, B. Champagne, A. Chardon and G. Berionni, *Angew. Chem. Int. Ed.*, 2022, **61**, e202112342.
51. A. Osi, N. Tumanov, J. Wouters, A. Chardon and G. Berionni, *Synthesis*, 2022, **55**, 347-353.
52. M. Yasuda, S. Yoshioka, S. Yamasaki, T. Somyo, K. Chiba and A. Baba, *Org. Lett.*, 2006, **8**, 761-764.
53. H. Zhu and E. Y. X. Chen, *Inorg. Chem.*, 2007, **46**, 1481-1487.
54. H. Braunschweig and R. D. Dewhurst, *Dalton Trans.*, 2011, **40**, 549-558.
55. N. Wiberg, K. Amelunxen, T. Blank, H.-W. Lerner, K. Polborn, H. Nöth, R. Littger, M. Rackl, M. Schmidt-Amelunxen, H. Schwenk-Kircher and M. Warchold, *Zeitschrift für Naturforschung B*, 2001, **56**, 634-651.
56. K. Huang, J. L. Dutton and C. D. Martin, *Chem. Eur. J.*, 2017, **23**, 10532-10535.
57. W. Lv, Y. Dai, R. Guo, Y. Su, D. A. Ruiz, L. L. Liu, C.-H. Tung and L. Kong, *Angew. Chem. Int. Ed.*, **n/a**, e202308467.
58. D. Tanaka, Y. Kadonaga, Y. Manabe, K. Fukase, S. Sasaya, H. Maruyama, S. Nishimura, M. Yanagihara, A. Konishi and M. Yasuda, *Journal of the American Chemical Society*, 2019, **141**, 17466-17471.
59. P. Wang, M. Zhang and C. Zhu, *Organometallics*, 2020, **39**, 2732-2738.
60. W. Wang, M. Bao, Y. Dai, X. Liu, C. Liu, C. Liu, Y. Su and X. Wang, *Organometallics*, 2022, **41**, 680-685.
61. T. M. Bass, C. R. Carr, T. J. Sherbow, J. C. Fettinger and L. A. Berben, *Inorg. Chem.*, 2020, **59**, 13517-13523.
62. E. J. Thompson, T. W. Myers and L. A. Berben, *Angew. Chem. Int. Ed.*, 2014, **53**, 14132-14134.
63. T. W. Myers and L. A. Berben, *Journal of the American Chemical Society*, 2013, **135**, 9988-9990.
64. C. L. Shaves, N. Villegas-Escobar, E. R. Clark and I. M. Riddlestone, *Chem. Eur. J.*, 2023, **29**.
65. L. M. Sigmund, E. Engels, N. Richert and L. Greb, *Chem. Sci.*, 2022, **13**, 11215-11220.
66. D. Roth, H. Wadepohl and L. Greb, *Angew. Chem. Int. Ed.*, 2020, **59**, 20930-20934.
67. L. M. Sigmund, R. Maier and L. Greb, *Chem. Sci.*, 2022, **13**, 510-521.
68. F. Ebner, L. M. Sigmund and L. Greb, *Angew. Chem. Int. Ed.*, 2020, **59**, 17118-17124.
69. F. Schön, L. M. Sigmund, F. Schneider, D. Hartmann, M. A. Wiebe, I. Manners and L. Greb, *Angew. Chem. Int. Ed.*, 2022, **61**, e202202176.
70. J. H. van't Hoff, *Arch. Neerl. Sci. Exactes Nat*, 1874, **9**, 445-454.
71. J. A. Le Bel, *Bull. Soc. Chim. Fr*, 1874, **22**, 337-347.

72. R. Keese, *Chem. Rev.*, 2006, **106**, 4787-4808.
73. D. Röttger and G. Erker, *Angewandte Chemie International Edition in English*, 1997, **36**, 812-827.
74. L.-M. Yang, E. Ganz, Z. Chen, Z.-X. Wang and P. v. R. Schleyer, *Angew. Chem. Int. Ed.*, 2015, **54**, 9468-9501.
75. G. Merino, M. A. Méndez-Rojas, A. Vela and T. Heine, *J. Comput. Chem.*, 2007, **28**, 362-372.
76. V. Vassilev-Galindo, S. Pan, K. J. Donald and G. Merino, *Nature Reviews Chemistry*, 2018, **2**, 0114.
77. R. Hoffmann, R. W. Alder and C. F. Wilcox, Jr., *Journal of the American Chemical Society*, 1970, **92**, 4992-4993.
78. F. A. Cotton and M. Millar, *Journal of the American Chemical Society*, 1977, **99**, 7886-7891.
79. P. A. Wender, T. M. Dore and M. A. deLong, *Tetrahedron Lett.*, 1996, **37**, 7687-7690.
80. A. I. Boldyrev, P. von Ragué Schleyer and R. Keese, *Mendeleev Commun.*, 1992, **2**, 93-95.
81. K. Yoshizawa and A. Suzuki, *Chem. Phys.*, 2001, **271**, 41-54.
82. D. Szieberth, M. Takahashi and Y. Kawazoe, *The Journal of Physical Chemistry A*, 2009, **113**, 707-712.
83. Y. Zhang, C. Zhang, Y. Mo and Z. Cao, *Chem. Eur. J.*, 2021, **27**, 1402-1409.
84. V. S. Thimmakondu and K. Thirumoorthy, *Computational and Theoretical Chemistry*, 2019, **1157**, 40-46.
85. S.-D. Li, C.-Q. Miao, J.-C. Guo and G.-M. Ren, *Journal of the American Chemical Society*, 2004, **126**, 16227-16231.
86. M.-h. Wang, X. Dong, Z.-h. Cui, M. Orozco-Ic, Y.-h. Ding, J. Barroso and G. Merino, *Chem. Commun.*, 2020, **56**, 13772-13775.
87. L.-Q. Zhao, J.-C. Guo and H.-J. Zhai, *Physical Chemistry Chemical Physics*, 2022, **24**, 7068-7076.
88. L. M. Sigmund, C. Ehlert, G. Gryn'ova and L. Greb, *The Journal of Chemical Physics*, 2022, **156**.
89. S.-D. Li, G.-M. Ren and C.-Q. Miao, *Inorg. Chem.*, 2004, **43**, 6331-6333.
90. S.-D. Li, J.-C. Guo, C.-Q. Miao and G.-M. Ren, *The Journal of Physical Chemistry A*, 2005, **109**, 4133-4136.
91. S.-D. Li and C.-Q. Miao, *The Journal of Physical Chemistry A*, 2005, **109**, 7594-7597.
92. T. N. Gribanova, R. M. Minyaev and V. I. Minkin, *Russ. J. Gen. Chem.*, 2005, **75**, 1651-1658.
93. P. v. R. Schleyer and A. E. Reed, *Journal of the American Chemical Society*, 1988, **110**, 4453-4454.
94. M.-J. Sun, X. Cao and Z. Cao, *Nanoscale*, 2018, **10**, 10450-10458.
95. J. Xu and Y.-h. Ding, *J. Comput. Chem.*, 2015, **36**, 355-360.
96. J.-C. Guo, C.-Q. Miao and G.-M. Ren, *Computational and Theoretical Chemistry*, 2014, **1032**, 7-11.
97. Y. Li, F. Li, Z. Zhou and Z. Chen, *Journal of the American Chemical Society*, 2011, **133**, 900-908.
98. W. Tiznado, N. Perez-Peralta, R. Islas, A. Toro-Labbe, J. M. Ugalde and G. Merino, *Journal of the American Chemical Society*, 2009, **131**, 9426-9431.
99. J.-C. Guo and S.-D. Li, *Journal of Molecular Structure: THEOCHEM*, 2007, **816**, 59-65.
100. Y. Wang, Y. Li and Z. Chen, *Acc. Chem. Res.*, 2020, **53**, 887-895.
101. C. Zhang, Z. Tian and W. Jia, *The Journal of Physical Chemistry A*, 2021, **125**, 843-847.
102. S. Durmaz, J. N. Murrell and J. B. Pedley, *J. Chem. Soc., Chem. Commun.*, 1972, DOI: 10.1039/C39720000933, 933-934.
103. D. C. Crans and J. P. Snyder, *Journal of the American Chemical Society*, 1980, **102**, 7152-7154.
104. M. J. M. Pepper, I. Shavitt, P. V. R. Schleyer, M. N. Glukhovtsev, R. Janoschek and M. Quack, *J. Comput. Chem.*, 1995, **16**, 207-225.
105. M. S. Gordon and M. W. Schmidt, *Journal of the American Chemical Society*, 1993, **115**, 7486-7492.
106. R. Schwarz and W. Kuchen, *Z. Anorg. Allg. Chem.*, 1951, **266**, 185-192.
107. H. Meyer and G. Nagorsen, *Angewandte Chemie International Edition in English*, 1979, **18**, 551-553.

108. E.-U. Würthwein and P. von Ragué Schleyer, *Angewandte Chemie International Edition in English*, 1979, **18**, 553-554.
109. J. D. Dunitz, *Angewandte Chemie International Edition in English*, 1980, **19**, 1034-1034.
110. D. Hartmann, T. Thorwart, R. Müller, J. Thusek, J. Schwabedissen, A. Mix, J.-H. Lamm, B. Neumann, N. W. Mitzel and L. Greb, *Journal of the American Chemical Society*, 2021, **143**, 18784-18793.
111. B. Ding, R. Keese and H. Stoeckli-Evans, *Angew. Chem. Int. Ed.*, 1999, **38**, 375-376.
112. G. Rong, R. Keese and H. Stoeckli-Evans, *Eur. J. Inorg. Chem.*, 1998, **1998**, 1967-1973.
113. M. Driess, N. Muresan and K. Merz, *Angew. Chem. Int. Ed.*, 2005, **44**, 6738-6741.
114. N. Kramer, C. Jöst, A. Mackenroth and L. Greb, *Chem. Eur. J.*, 2017, **23**, 17764-17774.
115. A. I. Boldyrev, X. Li and L.-S. Wang, *Angew. Chem. Int. Ed.*, 2000, **39**, 3307-3310.
116. T. Nukazawa and T. Iwamoto, *Journal of the American Chemical Society*, 2020, **142**, 9920-9924.
117. P. Ghana, J. Rump, G. Schnakenburg, M. I. Arz and A. C. Filippou, *Journal of the American Chemical Society*, 2021, **143**, 420-432.
118. F. Ebner and L. Greb, *Journal of the American Chemical Society*, 2018, **140**, 17409-17412.
119. F. Ebner and L. Greb, *Chem*, 2021, **7**, 2151-2159.
120. C. Shan, S. Dong, S. Yao, J. Zhu and M. Driess, *Journal of the American Chemical Society*, 2023, **145**, 7084-7089.
121. A. Sekiguchi, T. Tanaka, M. Ichinohe, K. Akiyama and S. Tero-Kubota, *Journal of the American Chemical Society*, 2003, **125**, 4962-4963.
122. N. Wiberg, W. Niedermayer, H. Nöth, J. Knizek, W. Ponikwar, K. Polborn, D. Fenske and G. Baum, *Z. Anorg. Allg. Chem.*, 2001, **627**, 594-606.
123. H. Tanaka, M. Ichinohe and A. Sekiguchi, *Journal of the American Chemical Society*, 2012, **134**, 5540-5543.
124. N. Weyer, M. Heinz, J. I. Schweizer, C. Bruhn, M. C. Holthausen and U. Siemeling, *Angew. Chem. Int. Ed.*, 2021, **60**, 2624-2628.
125. N. Weyer, C. Bruhn and U. Siemeling, *Zeitschrift für Naturforschung B*, 2023, **78**, 421-426.
126. R. Guthardt, H. L. Jacob, D. Herle, M. Leibold, C. Bruhn, M. Heinz, M. C. Holthausen and U. Siemeling, *Chemistry – An Asian Journal*, 2023, **18**, e202300266.
127. M. Driess, N. Dona and K. Merz, *Chemistry – A European Journal*, 2004, **10**, 5971-5976.
128. G. Bettermann and A. J. Arduengo, *Journal of the American Chemical Society*, 1988, **110**, 877-879.
129. J. Henning, H. Schubert, K. Eichele, F. Winter, R. Pöttgen, H. A. Mayer and L. Wesemann, *Inorg. Chem.*, 2012, **51**, 5787-5794.
130. S. Khan, R. Michel, J. M. Dieterich, R. A. Mata, H. W. Roesky, J.-P. Demers, A. Lange and D. Stalke, *Journal of the American Chemical Society*, 2011, **133**, 17889-17894.
131. J. Flock, A. Suljanovic, A. Torvisco, W. Schoefberger, B. Gerke, R. Pöttgen, R. C. Fischer and M. Flock, *Chem. Eur. J.*, 2013, **19**, 15504-15517.
132. T. Chu, L. Belding, A. van der Est, T. Dudding, I. Korobkov and G. I. Nikonov, *Angew. Chem. Int. Ed.*, 2014, **53**, 2711-2715.
133. M. T. Nguyen, D. Gusev, A. Dmitrienko, B. M. Gabidullin, D. Spasyuk, M. Pilkington and G. I. Nikonov, *Journal of the American Chemical Society*, 2020, **142**, 5852-5861.
134. A. a. Swidan, P. B. J. St. Onge, J. F. Binder, R. Suter, N. Burford and C. L. B. Macdonald, *Dalton Trans.*, 2019, **48**, 7835-7843.
135. H. Ruppert and L. Greb, *Angew. Chem. Int. Ed.*, 2022, **61**, e202116615.
136. X. Liu, Y. Dai, M. Bao, W. Wang, Q. Li, C. Liu, X. Wang and Y. Su, *Chem. Sci.*, 2023, DOI: 10.1039/D2SC07006E.
137. R. Yadav, P. Janßen, M. Schorpp and L. Greb, *Journal of the American Chemical Society*, 2023, DOI: 10.1021/jacs.3c04424.

138. H. Fang, H. Jing, A. Zhang, H. Ge, Z. Yao, P. J. Brothers and X. Fu, *Journal of the American Chemical Society*, 2016, **138**, 7705-7710.
139. H. Jing, H. Ge, C. Li, Y. Jin, Z. Wang, C. Du, X. Fu and H. Fang, *Organometallics*, 2019, **38**, 2412-2416.
140. A. Brand and W. Uhl, *Chem. Eur. J.*, 2019, **25**, 1391-1404.
141. S. A. Culley and A. J. Arduengo, III, *Journal of the American Chemical Society*, 1984, **106**, 1164-1165.
142. A. J. Arduengo, III and C. A. Stewart, *Chemical Reviews*, 1994, **94**, 1215-1237.
143. D. Houalla, F. H. Osman, M. Sanchez and R. Wolf, *Tetrahedron Lett.*, 1977, **18**, 3041-3044.
144. C. Bonningue, D. Houalla, M. Sanchez, R. Wolf and F. H. Osman, *Journal of the Chemical Society, Perkin Transactions 2*, 1981, DOI: 10.1039/P29810000019, 19-25.
145. R. Wolf, *Pure Appl. Chem.*, 1980, **52**, 1141-1150.
146. G. Baccolini, E. Mezzina and P. E. Todesco, *J. Chem. Soc., Perkin Trans. 1*, 1988, DOI: 10.1039/P19880003281, 3281-3283.
147. G. Baccolini, C. A. Mosticchio, E. Mezzina, C. Rizzoli and P. Sgarabotto, *Heteroat. Chem*, 1993, **4**, 319-322.
148. C. Camacho-Camacho, F. J. Martínez-Martínez, M. D. J. Rosales-Hoz and R. Contreras, *Phosphorus, Sulfur, and Silicon and the Related Elements*, 1994, **91**, 189-203.
149. A. Murillo, L. M. Chiquete, P. Josephnathan and R. Contreras, *Phosphorus, Sulfur, and Silicon and the Related Elements*, 1990, **53**, 87-101.
150. S. Lochschmidt and A. Schmidpeter, *Zeitschrift für Naturforschung B*, 1985, **40**, 765-773.
151. J. Abbenseth and J. M. Goicoechea, *Chemical Science*, 2020, **11**, 9728-9740.
152. L. Dostál, *Coord. Chem. Rev.*, 2017, **353**, 142-158.
153. M. Driess, J. Aust, K. Merz and C. van Wüllen, *Angew. Chem. Int. Ed.*, 1999, **38**, 3677-3680.
154. D. W. Stephan, *Angew. Chem. Int. Ed.*, 2000, **39**, 501-502.
155. J. Hyvl, W. Y. Yoshida, A. L. Rheingold, R. P. Hughes and M. F. Cain, *Chem. Eur. J.*, 2016, **22**, 17562-17565.
156. P. Šimon, F. de Proft, R. Jambor, A. Růžička and L. Dostál, *Angew. Chem. Int. Ed.*, 2010, **49**, 5468-5471.
157. I. Vránová, M. Alonso, R. Lo, R. Sedlák, R. Jambor, A. Růžička, F. D. Proft, P. Hobza and L. Dostál, *Chem. Eur. J.*, 2015, **21**, 16917-16928.
158. A. J. Arduengo, D. A. Dixon and D. C. Roe, *Journal of the American Chemical Society*, 1986, **108**, 6821-6823.
159. D. G. Gilheany, *Chem. Rev.*, 1994, **94**, 1339-1374.
160. S. Kundu, *Chemistry – An Asian Journal*, 2020, **15**, 3209-3224.
161. P. P. Power, *Nature*, 2010, **463**, 171-177.
162. M. Driess, N. Muresan, K. Merz and M. Päch, *Angew. Chem. Int. Ed.*, 2005, **44**, 6734-6737.
163. N. L. Dunn, M. Ha and A. T. Radosevich, *Journal of the American Chemical Society*, 2012, **134**, 11330-11333.
164. G. Zeng, S. Maeda, T. Taketsugu and S. Sakaki, *ACS Catalysis*, 2016, **6**, 4859-4870.
165. G. Zeng, S. Maeda, T. Taketsugu and S. Sakaki, *Angew. Chem. Int. Ed.*, 2014, **53**, 4633-4637.
166. S. M. McCarthy, Y.-C. Lin, D. Devarajan, J. W. Chang, H. P. Yennawar, R. M. Rioux, D. H. Ess and A. T. Radosevich, *Journal of the American Chemical Society*, 2014, **136**, 4640-4650.
167. A. Pal and K. Vanka, *Inorg. Chem.*, 2016, **55**, 558-565.
168. W. Zhao, S. M. McCarthy, T. Y. Lai, H. P. Yennawar and A. T. Radosevich, *Journal of the American Chemical Society*, 2014, **136**, 17634-17644.
169. S. Lim and A. T. Radosevich, *Journal of the American Chemical Society*, 2020, **142**, 16188-16193.
170. K. Lee, A. V. Blake, A. Tanushi, S. M. McCarthy, D. Kim, S. M. Loria, C. M. Donahue, K. D. Spielvogel, J. M. Keith, S. R. Daly and A. T. Radosevich, *Angew. Chem. Int. Ed.*, 2019, **58**, 6993-6998.

171. A. Tanushi and A. T. Radosevich, *Journal of the American Chemical Society*, 2018, **140**, 8114-8118.
172. Y.-C. Lin, E. Hatzakis, S. M. McCarthy, K. D. Reichl, T.-Y. Lai, H. P. Yennawar and A. T. Radosevich, *Journal of the American Chemical Society*, 2017, **139**, 6008-6016.
173. J. Cui, Y. Li, R. Ganguly, A. Inthirarajah, H. Hirao and R. Kinjo, *Journal of the American Chemical Society*, 2014, **136**, 16764-16767.
174. J. Cui, Y. Li, R. Ganguly and R. Kinjo, *Chem. Eur. J.*, 2016, **22**, 9976-9985.
175. A. Hentschel, A. Brand, P. Wegener and W. Uhl, *Angew. Chem. Int. Ed.*, 2018, **57**, 832-835.
176. A. Brand, P. Wegener, A. Hepp and W. Uhl, *Organometallics*, 2020, **39**, 1384-1392.
177. T. P. Robinson, D. M. De Rosa, S. Aldridge and J. M. Goicoechea, *Angewandte Chemie International Edition*, 2015, **54**, 13758-13763.
178. T. P. Robinson, D. De Rosa, S. Aldridge and J. M. Goicoechea, *Chem. Eur. J.*, 2017, **23**, 15455-15465.
179. T. P. Robinson, S.-K. Lo, D. De Rosa, S. Aldridge and J. M. Goicoechea, *Chem. Eur. J.*, 2016, **22**, 15712-15724.
180. J. Abbenseth, O. P. E. Townrow and J. M. Goicoechea, *Angewandte Chemie International Edition*, 2021, **60**, 23625-23629.
181. A. J. King, J. Abbenseth and J. M. Goicoechea, *Chem. Eur. J.*, 2023, **29**, e202300818.
182. S. Volodarsky and R. Dobrovetsky, *Chemical Communications*, 2018, **54**, 6931-6934.
183. S. Volodarsky, D. Bawari and R. Dobrovetsky, *Angew. Chem. Int. Ed.*, 2022, **61**, e202208401.
184. D. Bawari, S. Volodarsky, Y. Ginzburg, K. Jaiswal, P. Joshi and R. Dobrovetsky, *Chem. Commun.*, 2022, **58**, 12176-12179.
185. S. Volodarsky, I. Malahov, D. Bawari, M. Diab, N. Malik, B. Tumanskii and R. Dobrovetsky, *Chem. Sci.*, 2022, **13**, 5957-5963.
186. S. B. H. Karnbrock, C. Golz, R. A. Mata and M. Alcarazo, *Angew. Chem. Int. Ed.*, 2022, **61**, e202207450.
187. K. Chulsky, I. Malahov, D. Bawari and R. Dobrovetsky, *Journal of the American Chemical Society*, 2023, **145**, 3786-3794.
188. A. D. Obi, D. A. Dickie, W. Tiznado, G. Frenking, S. Pan and R. J. Gilliard, Jr., *Inorg. Chem.*, 2022, **61**, 19452-19462.
189. H. W. Moon and J. Cornella, *ACS Catalysis*, 2022, **12**, 1382-1393.
190. F. Wang, O. Planas and J. Cornella, *Journal of the American Chemical Society*, 2019, **141**, 4235-4240.
191. M. Hejda, R. Jirásko, A. Růžička, R. Jambor and L. Dostál, *Organometallics*, 2020, **39**, 4320-4328.
192. P. Šimon, R. Jambor, A. Růžička and L. Dostál, *Organometallics*, 2013, **32**, 239-248.
193. J. Zechovský, E. Kertész, V. Kremláček, M. Hejda, T. Mikysek, M. Erben, A. Růžička, R. Jambor, Z. Benkő and L. Dostál, *Organometallics*, 2022, **41**, 2535-2550.
194. G. Wang, L. A. Freeman, D. A. Dickie, R. Mokrai, Z. Benkő and R. J. Gilliard Jr., *Chemistry – A European Journal*, 2019, **25**, 4335-4339.
195. Y. Pang, M. Leutzsch, N. Nöthling and J. Cornella, *Journal of the American Chemical Society*, 2020, **142**, 19473-19479.
196. M. Mato, D. Spinnato, M. Leutzsch, H. W. Moon, E. J. Reijerse and J. Cornella, *Nature Chemistry*, 2023, **15**, 1138-1145.
197. A. J. Arduengo, III, C. A. Stewart, F. Davidson, D. A. Dixon, J. Y. Becker, S. A. Culley and M. B. Mizen, *Journal of the American Chemical Society*, 1987, **109**, 627-647.
198. C. A. Stewart, R. L. Harlow and A. J. Arduengo III, *Journal of the American Chemical Society*, 1985, **107**, 5543-5544.
199. S. A. Culley and A. J. Arduengo III, *Journal of the American Chemical Society*, 1985, **107**, 1089-1090.
200. A. J. Arduengo, C. A. Stewart and F. Davidson, *Journal of the American Chemical Society*, 1986, **108**, 322-323.

201. M. K. Mondal, L. Zhang, Z. Feng, S. Tang, R. Feng, Y. Zhao, G. Tan, H. Ruan and X. Wang, *Angewandte Chemie International Edition*, 2019, **58**, 15829-15833.
202. K. M. Marczenko, J. A. Zurakowski, M. B. Kindervater, S. Jee, T. Hynes, N. Roberts, S. Park, U. Werner-Zwanziger, M. Lumsden, D. N. Langelaan and S. S. Chitnis, *Chemistry – A European Journal*, 2019, **25**, 16414-16424.
203. M. B. Kindervater, K. M. Marczenko, U. Werner-Zwanziger and S. S. Chitnis, *Angew. Chem. Int. Ed.*, 2019, **58**, 7850-7855.
204. C. A. Stewart, J. C. Calabrese and A. J. Arduengo, III, *Journal of the American Chemical Society*, 1985, **107**, 3397-3398.
205. M. Gimferrer, S. Danés, D. M. Andrada and P. Salvador, *Inorg. Chem.*, 2021, **60**, 17657-17668.
206. K. M. Marczenko, S. Jee and S. S. Chitnis, *Organometallics*, 2020, **39**, 4287-4296.
207. T. J. Hannah, W. M. McCarvell, T. Kirsch, J. Bedard, T. Hynes, J. Mayho, K. L. Bamford, C. W. Vos, C. M. Kozak, T. George, J. D. Masuda and S. S. Chitnis, *Chem. Sci.*, 2023, **14**, 4549-4563.
208. T. Hynes, J. D. Masuda and S. S. Chitnis, *Chempluschem*, 2022, **In Press**, e202200244.
209. M. Schorpp, R. Yadav, D. Roth and L. Greb, *Angew. Chem. Int. Ed.*, 2022, **61**, e202207963.
210. C. M. Lemon, S. J. Hwang, A. G. Maher, D. C. Powers and D. G. Nocera, *Inorganic Chemistry*, 2018, **57**, 5333-5342.
211. R. M. Christie, A. S. Ingram, D. H. Reid and R. G. Webster, *J. Chem. Soc., Chem. Commun.*, 1973, DOI: 10.1039/C39730000092, 92-93.
212. D. H. Reid and R. G. Webster, *J. Chem. Soc., Perkin Trans. 1*, 1975, DOI: 10.1039/P19750000775, 775-780.
213. M. R. Detty and H. R. Luss, *The Journal of Organic Chemistry*, 1983, **48**, 5149-5151.
214. J. P. Jacobsen, J. Hansen, C. T. Pedersen and T. Pedersen, *Journal of the Chemical Society, Perkin Transactions 2*, 1979, DOI: 10.1039/P29790001521, 1521-1524.
215. E. Magdzinski, P. Gobbo, C. D. Martin, M. S. Workentin and P. J. Ragogna, *Inorg. Chem.*, 2012, **51**, 8425-8432.
216. C. D. Martin, C. M. Le and P. J. Ragogna, *Journal of the American Chemical Society*, 2009, **131**, 15126-15127.
217. C. D. Martin and P. J. Ragogna, *Inorg. Chem.*, 2012, **51**, 2947-2953.
218. C. Chatgilialoglu, A. L. Castelhano and D. Griller, *The Journal of Organic Chemistry*, 1985, **50**, 2516-2518.
219. C. W. Perkins, J. C. Martin, A. J. Arduengo, W. Lau, A. Alegria and J. K. Kochi, *Journal of the American Chemical Society*, 1980, **102**, 7753-7759.
220. Y. Imada, H. Nakano, K. Furukawa, R. Kishi, M. Nakano, H. Maruyama, M. Nakamoto, A. Sekiguchi, M. Ogawa, T. Ohta and Y. Yamamoto, *Journal of the American Chemical Society*, 2016, **138**, 479-482.
221. C. W. Perkins, R. B. Clarkson and J. C. Martin, *Journal of the American Chemical Society*, 1986, **108**, 3206-3210.
222. X. Zhou, X. Pang, L. Nie, C. Zhu, K. Zhuo, Q. Zhuo, Z. Chen, G. Liu, H. Zhang, Z. Lin and H. Xia, *Nat Commun*, 2019, **10**, 1488.
223. C. Zhu and H. Xia, *Acc. Chem. Res.*, 2018, **51**, 1691-1700.
224. G. Hum, S. J. I. Phang, H. C. Ong, F. León, S. Quek, Y. X. J. Khoo, C. Li, Y. Li, J. K. Clegg, J. Díaz, M. C. Stuparu and F. García, *Journal of the American Chemical Society*, 2023, **145**, 12475-12486.
225. F. García, J. M. Goodman, R. A. Kowenicki, I. Kuzu, M. McPartlin, M. A. Silva, L. Riera, A. D. Woods and D. S. Wright, *Chem. Eur. J.*, 2004, **10**, 6066-6072.
226. B. D. Rekken, T. M. Brown, J. C. Fettinger, F. Lips, H. M. Tuononen, R. H. Herber and P. P. Power, *Journal of the American Chemical Society*, 2013, **135**, 10134-10148.
227. N. J. Roberts, E. R. Johnson and S. S. Chitnis, *Organometallics*, 2022, **41**, 2180-2187.